CHAPTER 8   ANALYSIS OF CLIMATE CHANGE

8.1   Procedures of Climate Change Analysis

The weather varies widely every day, every month, and every year. The climate, which is the average behavior of the weather for a long period of time in a particular region, has presented rather unique stable patterns. A climate with stable patterns is the basis of a hydrologic study. The possible reoccurrence, in other words, is fundamental for the hydrologic study which relies on past hydrologic records.

The climate is changing naturally in the long term view. Human activities in the past 100 years have accelerated the rate of change significantly. The target year for the Water Security Plan (WSP) is 2040 and it is only 30 years away from now. However, it is not certain that the climate at that time will be the same as the present one. The study on climate change is therefore crucial to make the WSP adaptable to the climate in the future.

It is common understanding that emission of greenhouse gases has been one of the most influential human activity that has affected climate change. Accordingly, adoption of the emission scenario is the first assumption to forecast climate change.

A general circulation model (GCM) is the most hopeful and advanced tool to understand the climate and project future climate conditions. The GCMs have been developed in various countries and introduced in the Fourth Assessment Report (AR4) conducted by the Intergovernmental Panel on Climate Change (IPCC), and most of those data are archived by the Phase 3 of the Coupled Model Inter-comparison Project (CMIP3). This Study is to avail of the results of the GCMs.

Although the GCMs are accepted widely as the best physically based tool for devising climate scenarios, there is a considerable gap or bias between the local climate condition and the simulation results. In order to apply the GCMs results to the catchment scale, the bias correction was made based on the methodology propounded by Professor Koike of the University of Tokyo.

There are 17 GCMs that made the daily data sets available among the existing 24 GCMs. The daily data sets of GCMs are archived in the Data Integration and Analysis System (DIAS) of Japan as well as CMIP3. The daily data sets were provided to JICA from DIAS as part of the cooperation between the University of Tokyo Earth Observation Data Integration and Fusion Research Initiative (EDITORIA) and JICA.

Every GCM has its own future scenario which is different from those of other GCMs. Even the GCMs, which are classified as state-of-the-arts of technology, cannot project an assured future climate. This uncertainty of the future climate should be evaluated quantitatively. The multi-model ensemble analysis affords to evaluate the uncertainty of the future climate.

The work flow of the climate change analysis is shown below.
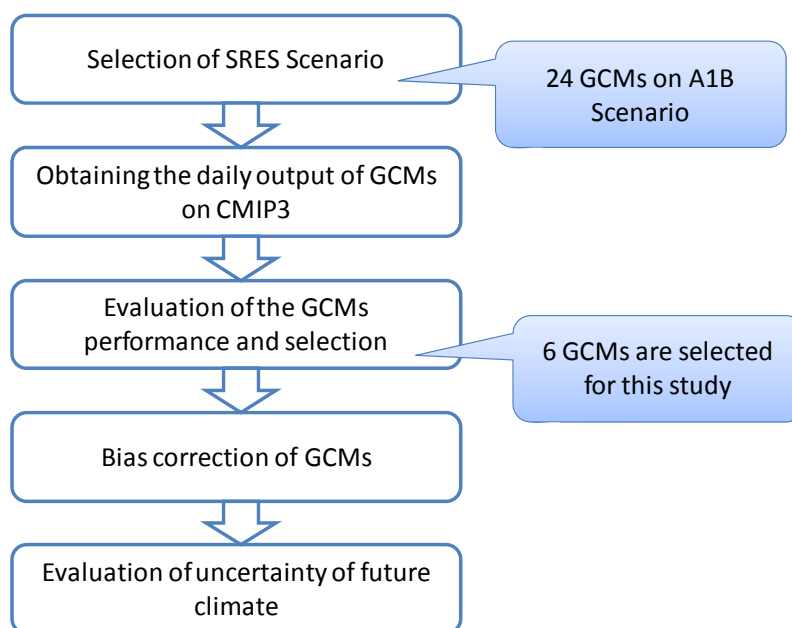
Source: JICA Study Team

Figure 8.1   Work Flow of the Climate Change Analysis

8.2 Selection of the Emission Scenario

In order to study the impact of climate change in the future, the concentrations of greenhouse gases and other pollutants in the atmosphere should be given as the boundary conditions for the numerical simulation models, to which climate is sensitive.

The Special Report on Emission Scenarios (SRES), published by the IPCC in 2000, describes the emissions scenarios that have been used to project the possible future climate change, for the IPCC Third Assessment Report (TAR) and in the IPCC Fourth Assessment Report (AR4). The report describes the future releases of greenhouse gases, aerosols, and other pollutants into the atmosphere together with information on land use and land cover. A set of four scenarios (A1, A2, B1, B2) have been developed. Each scenario describes one possible demographic, politico-economic, societal, and technological future. The SRES scenarios are tabulated below.

Table 8.1   SRES Scenarios

Scenario	SRES Emission Scenarios	CO_2 Stabilization
A1	A future world of very rapid economic growth, global population that peaks in mid-century and declines thereafter, and rapid introduction of new and more efficient technologies The A1 scenario develops into three groups that describe alternative directions of technological change in the energy system. -A1F1: fossil-intensive -A1T: non-fossil energy sources -A1B: balance across all sources	A1F1: Not stabilized A1T: 650 ppm A1B: 750 ppm
A2	A very heterogeneous world with continuously increasing global population and regionally oriented economic growth that is more fragmented and slower than in the other scenarios	Not stabilized

B1	A convergent world with the same global population as in the A1 storyline but with rapid changes in economic structures toward a service and information economy, with reduction in materials intensity, and the introduction of clean and resource-efficient technologies.	550 ppm
B2	A world in which the emphasis is on local solutions to economic, social, and environmental sustainability, with continuously increasing population (lower than A2) and intermediate economic development.	650 ppm

Source: Task Group on Data and Scenario Support for Impact and Climate Assessment (TGICA), IPCC

The scenario A1B was selected for this Study because it is physically plausible and consistent, and the potential range of future regional climate change is realistic. In addition, the most numbers of data set available among the SRES scenarios are on A1B scenario.

8.3 Global Circulation Models

Various institutes have developed GCMs to establish frameworks to forecast climate change focusing on their own purposes. The model outputs are available as mentioned before and selection of models which fit to the Study's purpose is imperative for climate change forecast.

Selection is based on the ability of the GCM to simulate the regional climate of the area in question. If a GCM is not able to reproduce the climatology of the region under study, it should be discarded and not to be used for further consideration. The selection of the domain is based on these broad synoptic scale phenomena. The climate phenomena, which are unique to the basins as well as the approximate areal coverage, should be accounted for.

At the basin scale, the selected GCMs should be able to reproduce the seasonal pattern of precipitation. In this respect, the correlation coefficient (Scorr) of grid data between that generated by the model and the current global dataset indicates the degree of fit of the model in terms of spatial variability. Meanwhile, the mean square root (RMSE) represents the general difference between those generated and the dataset developed based on the recorded data. The adopted global data set is GPCP in this Study to evaluate the similarities in the average monthly precipitations for both seasonal and spatial variability. Meanwhile, JRA25 output was the global dataset used to compare other meteorological variables.

To evaluate the GCMs' ability to represent the small-scale precipitation, additional screening should be done to eliminate the worst performing GCMs. The following three additional criteria were used to achieve this:

1) The long-term observed average rainfall (climatology) of the basin should be compared to the GCMs' outputs. If a GCM is not able to represent the seasonal variability, then it should be eliminated.

2) If the GCM produces unreasonably long continuous dry days after the no-rain correction, that model should be eliminated too.

3) Lastly, if the observed rainfall distribution within the basin is not uniformly distributed, the basin should be divided into sub-basins (based on areas with high rainfall, medium rainfall, small rainfall – usually related to elevation and land use) in the model selection comparison.

Selection of GCMs among available models in CMIP3 is crucial for this multi-model analysis. Most GCMs have problems with low rainfall intensity during heavy rainfall, low seasonal representation, and low intensity but long rainy days (drizzle). There are seven parameters considered in selecting the appropriate GCMs that comprises the ensemble. These parameters are precipitation, outgoing long wave radiation, sea surface temperature, sea level pressure, air temperature, meridional wind, and zonal wind.

The area considered for local scale meteorological parameter (precipitation) is bounded by 115^oE to 130^oE and, 10^oN to 20^oN. The area is shown in Figure 10.2.
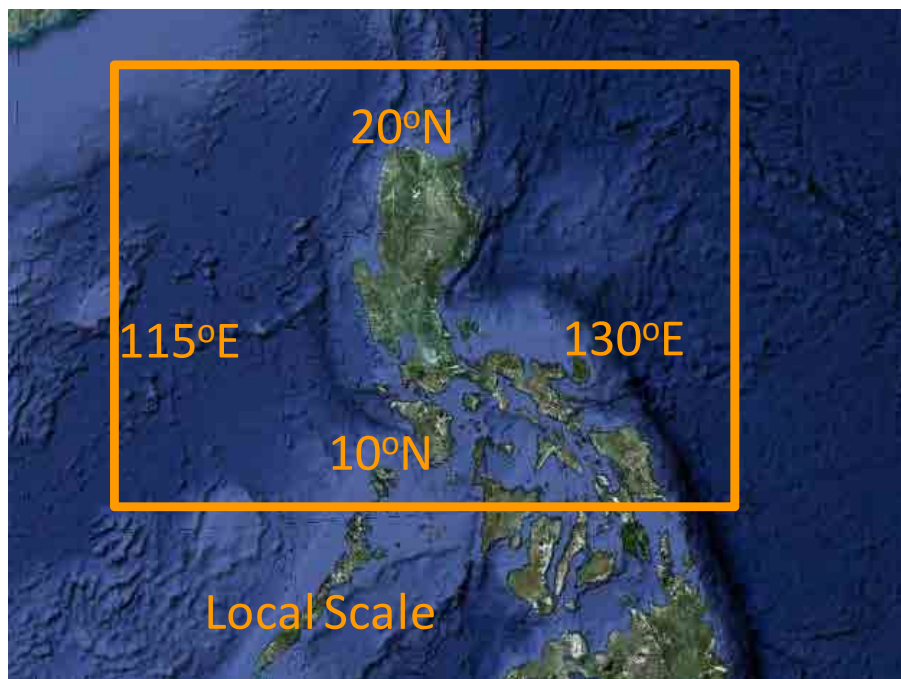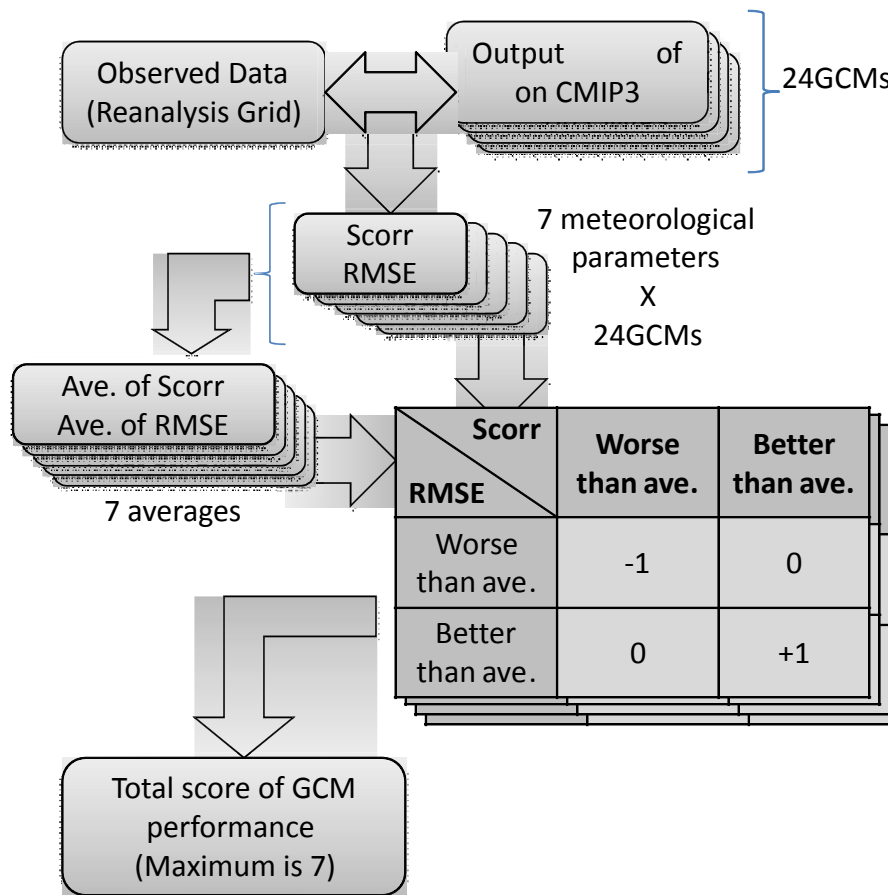

Source: JICA Study Team

Figure 8.2   Area Considered for the Local Scale Meteorological Parameter

For large scale circulations and surrounding oceans, the area considered is bounded by 80^oE to 160^oE and 0^oN to 20^oN. This includes the Bay of Bengal, Indian Ocean, Philippine Sea, and Java Sea. The following parameters considered are: sea level pressure, air temperature, meridional wind, zonal wind, outgoing long wave radiation, and sea surface temperature. This area was selected to account for the Asian summer monsoon, Southeast Asian summer monsoon (0^oN to 10^oN, 90^oE to 130^oE), Indian summer monsoon (5^oN to 20^oN, 40^oE to 80^oE), East Asian summer monsoon (20^oN to 45^oN, 110^oE to 140^oE).

In the Study Area, the seasonal reproducibility of GCMs is important for the development plan of the water management, so the spatial correlation (Scorr) and root mean square error (RMSE) for wet season, from March to November were considered. A simple index counter was used for the evaluation of the models and counting RMSE and scorr values for the meteorological parameter. If the scorr of a model is above the averages of the whole GCMs and the RMSE is smaller than the average, the rating of the model is 1. If the scorr is less than the average and RMSE is more than the average, -1 is assigned to the model. The score to be assigned is 0 in other cases. There are seven adopted meteorological parameters including rainfall. Priority is given to models that were selected for precipitation. Furthermore, the

seasonality of these models were checked and compared to the observed rainfall gauges. The schematic image of the procedure of GCM selection is shown in Figure 8.3.

Source: JICA Study Team

Figure 8.3   Procedure of the Scoring System for Evaluating GCMs Performance

Based on the scoring system, the following six GCMs were selected based on the steps described for further study:

✓   Screening 1: 16 GCMs, having daily data which are available, were passed.
✓   Screening 2: 13 GCMs, having positive grand total score for wet season, were passed.
✓   Screening 3: 6 GCMs, having a +1 score for the evaluation of precipitation reproducibility, were selected.

The selected GCMs were gfdl_cm2_0, gfdl_cm2_1, ipsl_cm4, giss_aom, ingv_echam4 and miroc3_2_medres. The screening process and the scores are shown in Table 8.2.

Table 8.2   The Screening Process and Selected GCMs

GCM	1st Screening	2nd Screening	3rd Screening	
	Daily Data Availability on CMIP3	**Ground Total Score for Wet Season (May - Nov)**	**Evaluation Score for Precipitation of Wet Season (May - Nov)**	**Selected**
gfdl_cm2_0		7	1	✔
gfdl_cm2_1		7	1	✔
cccma_cgcm3_1		5	0	
ipsl_cm4		5	1	✔
ncar_ccsm3_0	missing	*5*	*1*	
ukmo_hadgem1	missing	*5*	*0*	
bccr_bcm2_0	incomplete	*4*	*0*	
cccma_cgcm3_1_t63		4	-1	
giss_aom		4	1	✔
ingv_echam4		4	1	✔
csiro_mk3_0		3	0	
miub_echo_g	incomplete	*3*	*1*	
mpi_echam5		3	-1	
cnrm_cm3		2	0	
csiro_mk3_5		2	0	
miroc3_2_medres		2	1	✔
mri_cgcm2_3_2a		2	-1	
miroc3_2_hires		0	*0*	
giss_model_e_r		-1	*1*	
ukmo_hadcm3	missing	*-2*	*-1*	
iap_fgoals1_0_g		-4	*0*	
inmcm3_0	missing	*-5*	*0*	
giss_model_e_h	missing	*-6*	*0*	
ncar_pcm1	missing	*-6*	*-1*	

<div style="border:1px solid #000;background:#fde9d9;width:120px"> </div> Passed the screening

<div style="border:1px solid #000;background:#bfbfbf;width:120px"> </div> Excluded by previous screening

Source: JICA Study Team

8.4   **Bias Correction and Downscaling**

8.4.1 **Methodology**

GCMs are effective tools to predict future climate conditions. However, GCMs have a bias or error in simulating 20th century precipitation and temperature, and therefore, the outputs are available only after the bias is corrected for hydrological models in order to accurately assess the impact of the projected climate change for a particular basin. This is the reason why bias correction is necessary.

The common problems of the GCMs are as follows:

a) Large diversity of the outputs among models,
b) Low seasonal representation,
c) Low extreme heavy rainfall rate, and
d) Small number of non-rainy days but with long drizzles.

In order to alleviate the above problems, the statistical bias correction was conducted. The detailed methodology thereof is described in Section 8.4.3.

There is another significant issue in the application of GCMs output for the hydrological study of basin scale. The grid sizes of the GCMs are too coarse as compared with the target basin scale. The large grid sizes of the selected GCMs are about 250 km which can cover the whole Study Area in one grid. Spatial downscaling is an important process for the application of the GCMs output to the hydrological study, since the distribution of the precipitation has specific locality.

The grid daily rainfall data of present condition were estimated based on observed rainfall data at existing rainfall gauging stations. The downscaling was achieved by performing bias correction to match the GCM data to every respective grid rainfall data. The detailed process of the preparation of the grid rainfall from the observed rainfall is described in Section 8.4.2 below and the temperature grid data in Section 8.4.4.

8.4.2 Preparation of Grid Rainfall Data

The assumed line of 0.05° on both latitude and longitude defines a grid. Thus, a grid covers a area of approximately 5 km x 5 km. An estimated grid rainfall was the weighted mean of the nearest four-point rainfall data (observed data at rainfall gauging station). The weight is assumed to be the inverse of square of the distance from the grid to the gauging station. The rainfall data from the nearest four stations which have valid data for the target dates were used for the estimation. The grid rainfall data was interpolated using the following equation below:

$$r = \frac{\displaystyle\sum_{i=1}^{4} \frac{r_i}{l_i^2}}{\displaystyle\sum_{i=1}^{4} \frac{1}{l_i^2}}$$

where, $r =$ Grid rainfall depth [mm/day]
$r_i =$ Observed daily rainfall at rainfall station i [mm]
$l_i =$ Distance between rainfall station i and the grid [km]
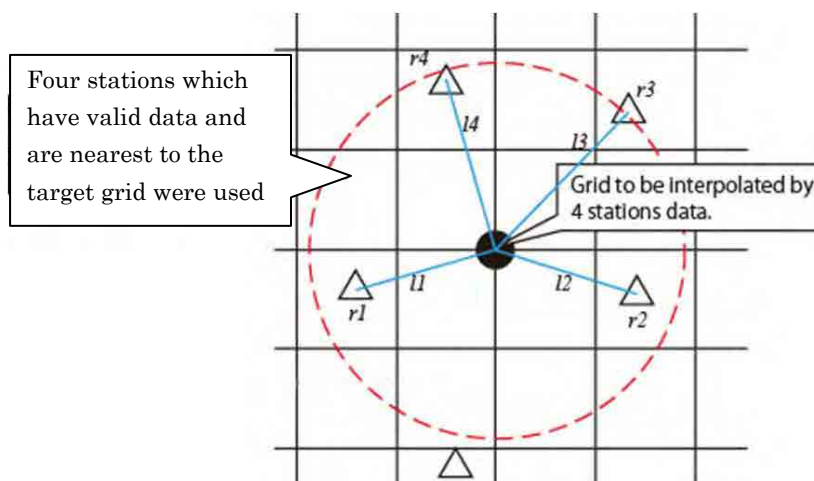
Source: JICA Study Team

Figure 8.4   Spatial Interpolation of Rainfall Data for Generating Grid Rainfall Data

The positive effects of generating the grid rainfall data are as follows:

- To fill up the missing data,
- To fill area of no rainfall station,
- To find the unreliable stations, and
- To compare with the output of the GCMs.

8.4.3   Bias Correction of Rainfall

It is well-known that the GCM precipitation output cannot be used to force the hydrological or other impact models without any prior bias correction if a more realistic output is desired (Ines and Hansen, 2006; Feddersen and Andersen, 2005; and Sharma et al., 2007). To utilize the GCM scenario output in a hydrological study, appropriate downscaling is needed. Two downscaling approaches are typically available, namely, the statistical downscaling and dynamic downscaling. Dynamic downscaling involves the use of finer resolution numerical weather prediction models with GCM output as the initial and boundary conditions. Statistical downscaling involves the use of statistical relationships to convert large-scale projections from GCM into finer spatial resolutions. This part of the report presents the necessary steps to achieve a simplified statistical approach based on the statistics over the Study Area.

To achieve a reasonable bias correction of precipitation, it is necessary to separately examine the bias in zero-rain days, normal rainy days, and extreme rainy days separately. Due to the difficulty in incorporating the microphysics schemes in the simulations, the GCMs tend to result in unreasonably large numbers of wet days (with lots of drizzle) and poor simulation of extreme events. This necessitates the separation of three said types of rainfall events. Moreover, bias correction should be performed separately for basins with extremely distinct seasons, e.g., very dry and wet seasons. This should be done at monthly or bi-monthly scales depending on the basin characteristics.

Bias correction using this approach covers a three-step process. The steps are for correcting tge numbers of dry days, normal days, and extreme rainy days as indicated in Figure 8.5.
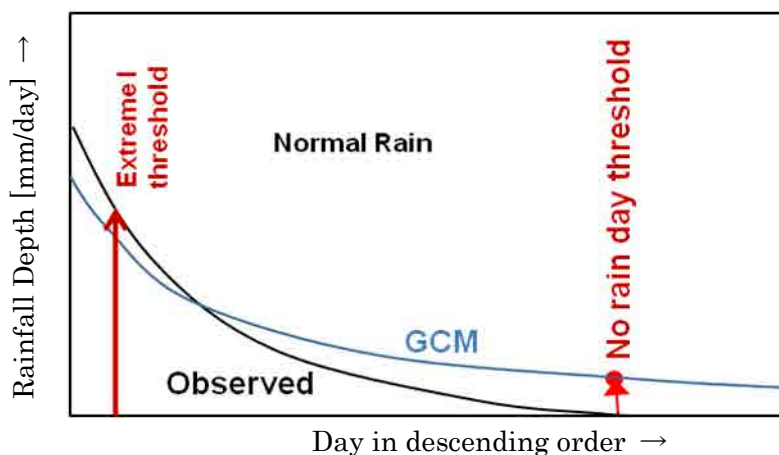
Source: JICA Study Team

Figure 8.5   Three Domains of Rainfall for Bias Correction

No-rain day correction

A common characteristic of all GCMs is the unreasonably large number of wet days, which is mostly represented by drizzle, and is probably attributable to lack of parameterization in GCMs. To correct this, the rank order approach is employed with procedure as follows:

1)   Both past observations and GCM generated values are ranked in descending order;

2)   A threshold of 0 mm/day in the observation is proposed as a no-rain day. The order or rank of this threshold is then used to determine the corresponding value of the no-rain day in the GCMs output;

3)   All the values equal or below this threshold in the GCM output are assumed to be zero; and

4)   No-rain day correction for the future GCM is to be based on the threshold for the past GCMs.

Extreme rainfall correction

Most of the GCMs underestimate extreme rainfall as compared with the observed rainfall. An appropriate correction on the values should be applied to fit with the distribution of the observed data.

Annual maximum rainfall values were selected for each year in the observed dataset. The lowest value of the annual maximum was selected as the threshold of the extreme events for the observed rainfall. Values above this threshold are defined as extreme events. The number of extreme events are determined from the observed data and set with the same number of extreme events in the past GCMs by ranking.

The appropriate probability distribution function (PDF) for the observed extreme rainfall and GCM outputs will be estimated. The difference between the PDFs is assumed to be the bias of the GCM for the extreme data. The relationship of the two PDFs can be considered as the bias correction function of the model output.

Normal rainfall correction

Normal rainfall is in the range between thresholds of zero rainfall and extreme rainfall. The normal rainfall data will be separated by month and sorted in descending order. The rank of rainfall can be regarded as a cumulative distribution function (CDF). The difference between the CDF of the observed data and that of the GCM indicates the bias for normal rainfall. The bias correction for normal rainfall will be done based on the relationship between CDFs of the observed and of the GCM output.

8.4.4 Bias Correction of Air Temperature

(1) Making Grid Temperature Data from Observed Record

Generally, the distribution of air temperature, which is greatly affected by elevation, does not have very strong locality. The assumed temperature variation rate of 0.6°C per 100 m in elevation was applied in this Study. The grid size was 0.05º in both latitude and longitude, and the size was the same as that of the grid rainfall data, which was generated in this Study. The procedures for the temperature data generation in grids are as follows:

1) Selection of the four nearest stations to the target grid point, which have valid data for the target date.
2) Obtain the elevation of the target grid point DEM data, wherein, Z_{grid} [El. m] is the elevation.
3) Correct the temperature of the surrounding stations ($T_{i\_observed}$) at the elevation of the target grid (Z_{grid}) from the elevation of the station (Z_i) using the temperature lapse rate, with the formula as follows:

$$T_{i\_corrected} = T_{i\_observed} + 0.006\,(Z_i - Z_{grid})$$

4) The temperature of the target grid (T_{grid}) is obtained by the spatial interpolation method, IDW, and the temperature data ($T_{i\_corrected}$) of the four nearest stations is corrected with the elevation of the target grid,

$$T_{grid} = \sum_{i=1}^{4} \frac{T_{i\_corrected}}{l_i} \Bigg/ \sum_{i=1}^{4} \frac{1}{l_i}$$

where, l_i: distance from station i to the target grid.

(2) Bias Correction of Air Temperature for the Output of Future GCMs

The CDFs were developed for the temperatures recorded and generated by the GCMs of the 20th Century Experiment (20C3M). Then, the relationship of the bias between the observed data and 20C3M was applied to the A1B data. The procedure of the bias correction is itemized as follows:

1) The GCMs grid data were adjusted to the grid of the observed temperature data.
2) The observed monthly mean temperature of the observed and the adjusted 20C3M temperature are estimated for the periods from 1981 to 2000.
3) All daily temperature data of a certain month are extracted and sorted in descending order. For example, the total number of daily temperature data in April for 20 years is 600.

4) For the ranking of temperature of 20C3M, the bias is considered as the gap between 20C3M and the observed data of the same rank.

5) The temperature of 20C3M was replaced by the observed data of the same rank of. Therefore, the bias-corrected monthly mean temperature of 20C3M must completely match with the observed.

6) The daily temperature of the A1B for 20 years, from 2046 to 2065, was processed in the same manner with the observed and 20C3M.

7) To correct the bias of the temperature of a particular rank, the gap between the 20C3M and the observed data of the same rank is added. This procedure is illustrated in Figure 8.6.
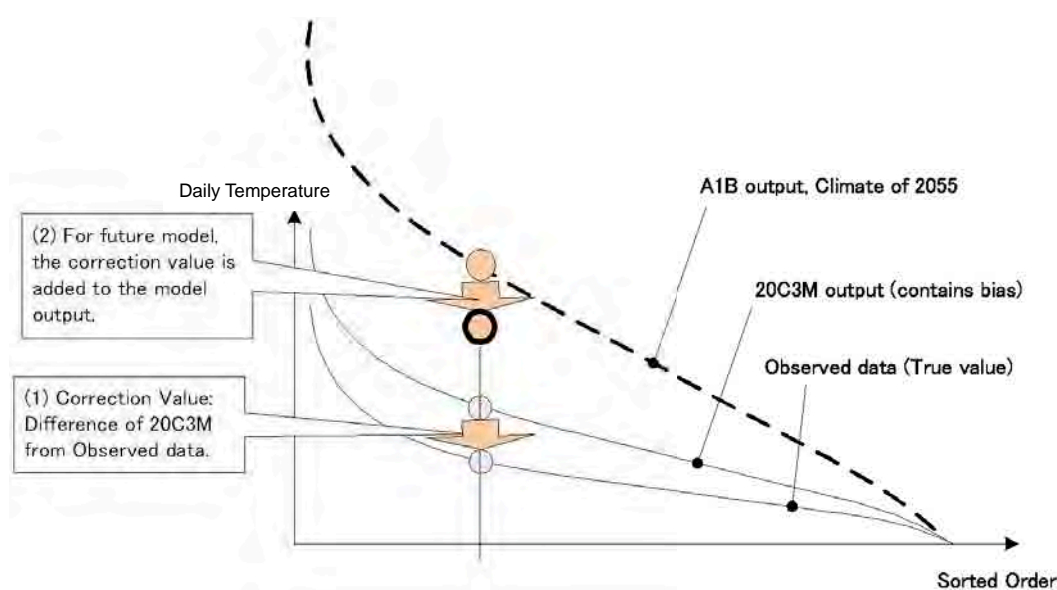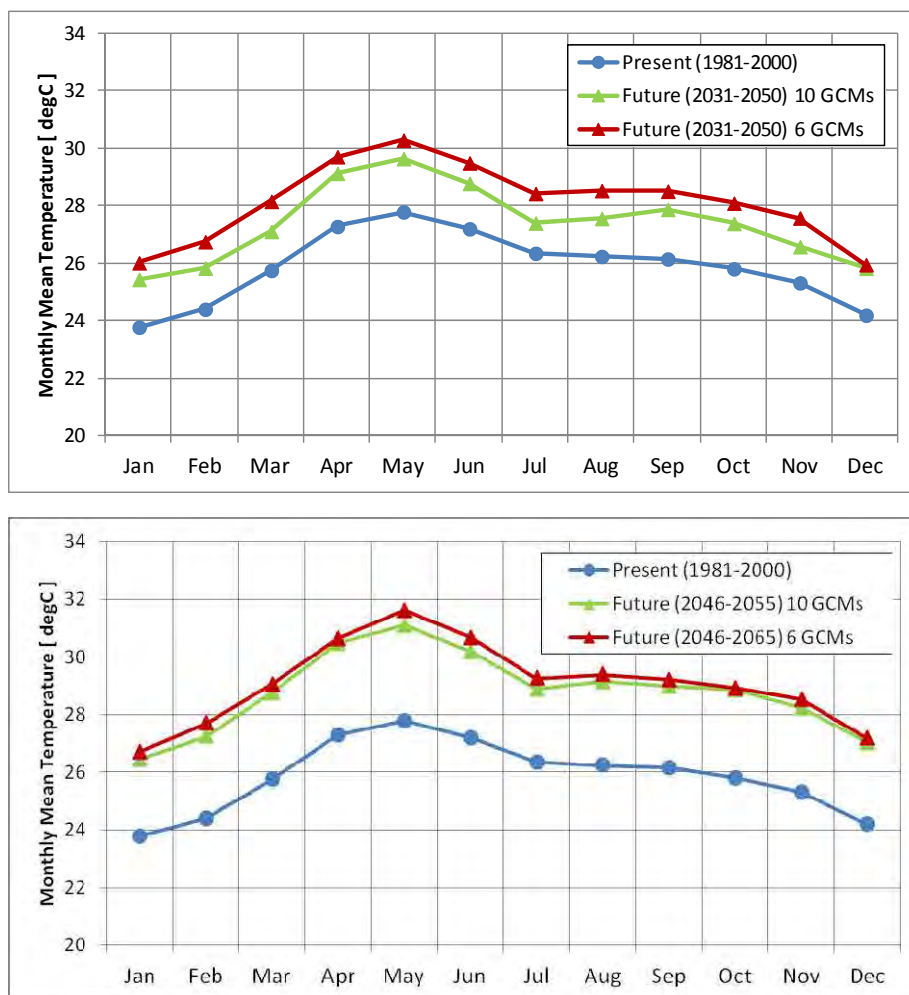

Source: JICA Study Team

Figure 8.6 Schematic Image of Bias Correction for the Output of A1B (2046-2065)

(3) Selection of GCMs for Temperature

The six GCMs were selected by evaluating the performance of the reproducibility of the present climatology. The performance of precipitation for the rainy season was prioritized for the GCM selection. The bias correction and projection for the target year were carried out for the six selected GCMs. The comparison of the ensemble mean air temperatures between the present and future conditions of 2040 and 2055 are shown in Figure 8.7, which are areal averages of the Pasig-Marikina Basin. It is easy to understand that air temperature will increase all over the target area in the future. However, the rise of 3ºC in 2055s seems to be extreme, and thus, deliberation is necessary.

The spatial correlation (Scorr) and RMSE between the climatologies of temperature of GCM and the observed data were evaluated, and the results are shown in Figure 8.8. The very wide diversity of GCM performance has emerged as shown in the figure and several models showed particularly poor performance. The GCMs that showed very bad performance were discarded. The selection processes were described in Table 8.3. The evaluated difference

between the present condition and the output of GCMs which were newly selected and prioritized according to temperature performance are shown in Figure 8.7. The rise of temperature was evaluated to be about 1.2°C in the target year from the present condition. This evaluation for temperature was considered in the evaluation of water demand for irrigation   water.

Source: JICA Study Team

Figure 8.7   Comparison of Air Temperature of Pasig-Marikina Basin Average Between the Ensemble Mean of the Six Selected GCMs Prioritizing on Precipitation Performance and the Ten Selected GCMs Prioritizing on Air Temperature Performance
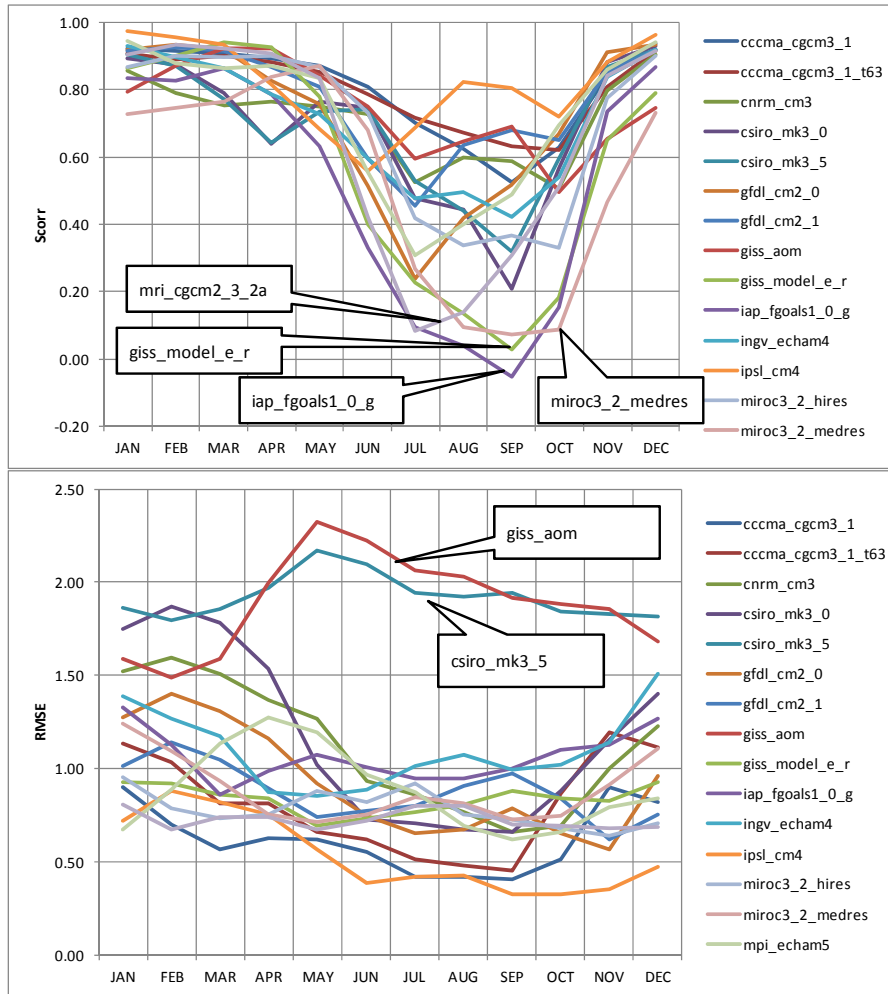
Source: JICA Study Team

Figure 8.8   GCMs Performance Evaluation of Air Temperature Reproducibility

**Table 8.3   Processes of GCMs' Selection for Temperature**

Model	Scorr	RMSE	Overall Evaluation	Current Selection
cccma_cgcm3_1	✔	✔	✔	
cccma_cgcm3_1_t63	✔	✔	✔	
cnrm_cm3	✔	✔	✔	
csiro_mk3_0	✔	✔	✔	✔
csiro_mk3_5	✔			
gfdl_cm2_0	✔	✔	✔	✔
gfdl_cm2_1	✔	✔	✔	✔
giss_aom	✔			
giss_model_e_r		✔		
iap_fgoals1_0_g		✔		
ingv_echam4	✔	✔	✔	✔
ipsl_cm4	✔	✔	✔	✔
miroc3_2_hires	✔	✔	✔	
miroc3_2_medres		✔		✔
mpi_echam5	✔	✔	✔	
mri_cgcm2_3_2a		✔		

Note: Selected GCMs are denoted by check marks. The GCMs were selected based on the index
             scorr and RMSE, as shown in the Overall Evaluation column. The Current Selection column
             shows the selected GCMs based on the rainfall performance.

Source: JICA Study Team

8.5   Projection to Target Year

The target year of this Study is 2040. The rainfall and temperature data for the period from 2031 to 2050 are necessary to assess the impacts of climate change. The simulated future daily data sets are available only from 2046 to 2065 for most GCMs. They do not cover the first 15 years from 2031 to 2045. There are two GCMs where daily data sets are available for the years 2021 to 2050. The periods of daily data availability of GCMs are shown in Figure 8.9.
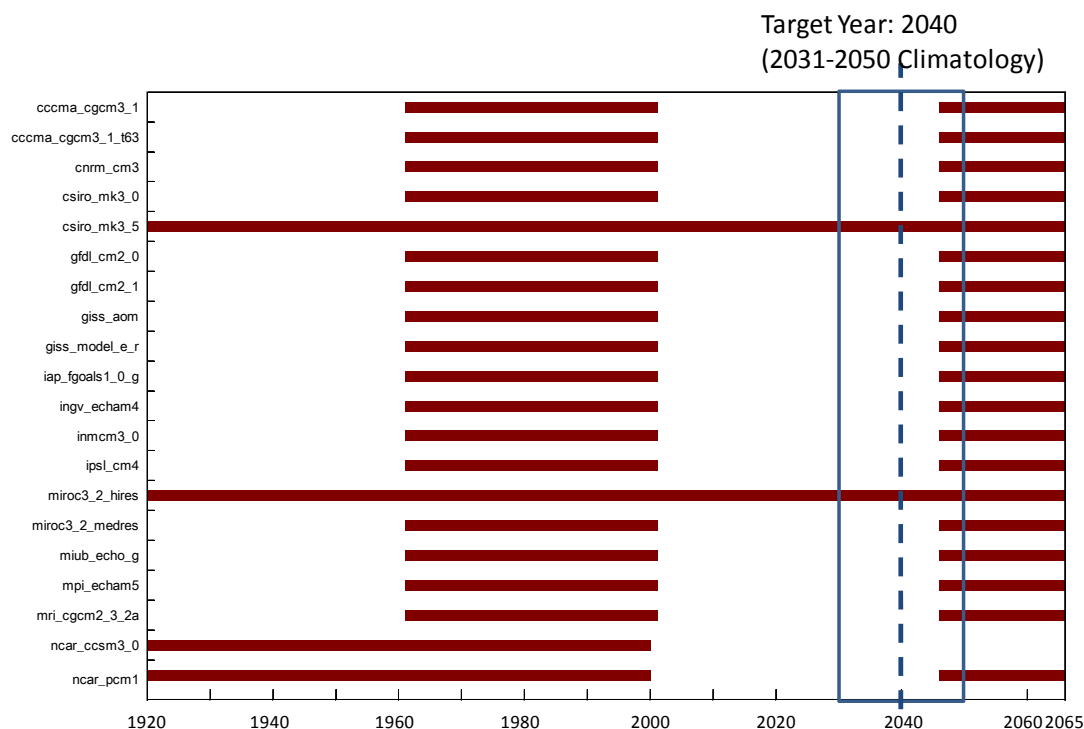
Source: JICA Study Team–Climate Change Impact Assessment and Runoff Simulation

Figure 8.9   Availability of Daily Data Set on CMIP3 and the Target Year of This Study

The other component of the Study, which is the "Climate Change Impact Assessment and Hydrological Simulation", recommended that the projection of hydrological condition in the 2040s (or from the years from 2031 to 2050) must to be conducted through the following steps:

1. The climatologies for the periods of 2031-2050 and 2046-2065 were compared using the data sets derived from the GCM csiro_mk3_5 and ncar_ccsm3_0, in which the 20-year data sets cover the target year.
2. The daily data sets are ranked from highest to lowest for 2031-2050 and 2046-2065. These were plotted in x-y scatter plots (x-axis for 2031-2050 and y-axis for 2046-2065).
3. The regression line was obtained from pairs of the two-period data.
4. The slope of the regression line can be applied to make the projected discharge data, which were obtained from the rainfall-runoff simulation with bias-corrected 2055 climate input data set.

The results of the regression analysis of the two GCMs having a continuing daily data for 2031-2065 are shown in Figure 8.10. The figures below are reprinted from the figures in the other report of this Study.
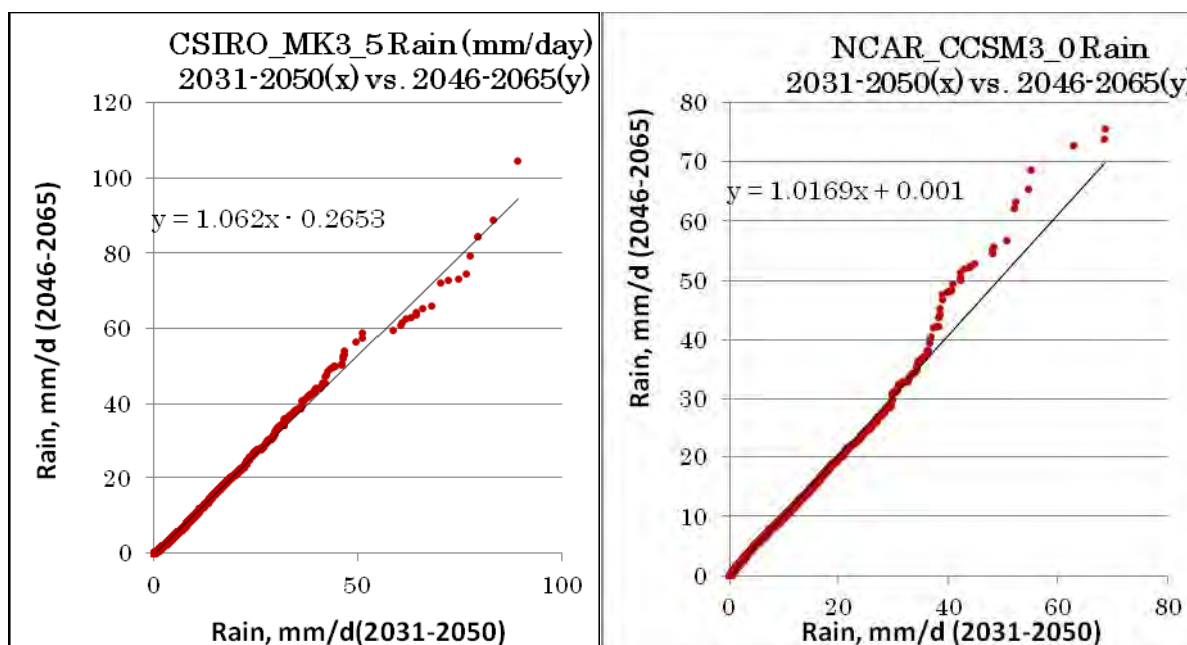
Source: JICA Study Team

Figure 8.10   Comparison Between the Daily Rainfall for Periods 2031-2050 and 2046-2065 of the Two GCMs Having Daily Data for 20 Years Including the Target Year

The monthly mean data sets for 2031-2050 are available for every GCM on the data distribution center of IPCC (http://www.ipcc-data.org). The main objective of the rainfall-runoff analysis is the quantitative evaluation of low water of the subjected rivers. The monthly scale of the time step for the water balance study is adequate. The result of comparison of the daily rainfall data set in 2031-2050 and 2046-2065, as presented in the report prepared by the other component, supports that the projection of the river discharge can be obtained by multiplying the ratios of the rainfall to the simulated river flow. Consequently, for this Study, the ratios which were obtained by the monthly average rainfall of two periods of the selected GCMs themselves were applied to the projection of the river flow to the target year. The detailed process and result are mentioned in Chapter 9.

8.6   Climate Change Impacts

8.6.1   Climate Change Impact on Rainfall

The bias correction of rainfall was implemented by the other component of the Study and the detailed procedure was explained in another report of this Study, which is the "Climate Change Impact Assessment and Hydrological Simulation". In order to clarify the impacts of climate change on rainfall, simple projection for monthly rainfall was conducted in this Study. The mean monthly rainfall for 20 years of the climate of the periods 2040s (years 2031-2050) and 2055s (2046-2065) were calculated, and the ratios for each month were applied to project the monthly mean rainfall to the target year.

The differences between the annual mean rainfall of the present (1981-2000), 2040s climate, and 2055s climate are summarized in Figure 8.11, and the seasonal comparisons are shown in Figures 8.12 and 8.13. In those figures, the future rainfall is the average of the bias-corrected rainfall of the six selected GCMs.

According to these figures, the annual rainfall is expected to increase in all over the subjected area from the present condition. The precipitation during the rainy season, which is from May to November, is expected to increase more than that in the dry season.

In the future, the amount of precipitation in the area facing the Philippine Sea is expected to be 500 mm/yr, which is 10-15% of the present annual rainfall of the area. The amount precipitation in the western half area of the Pampanga River basin is evaluated to be about 100 mm/yr, which is only 6% of the present annual rainfall. The increasing amounts of precipitation for the high rainfall area are expected to be higher than that of the low rainfall area. The difference between the increasing amounts of precipitation for 2040s and 2055s were not considered.

Present (1981-2000) 2040s (2031-2050) 2055s (2046-2065)

Present and 2040s Present and 2055s
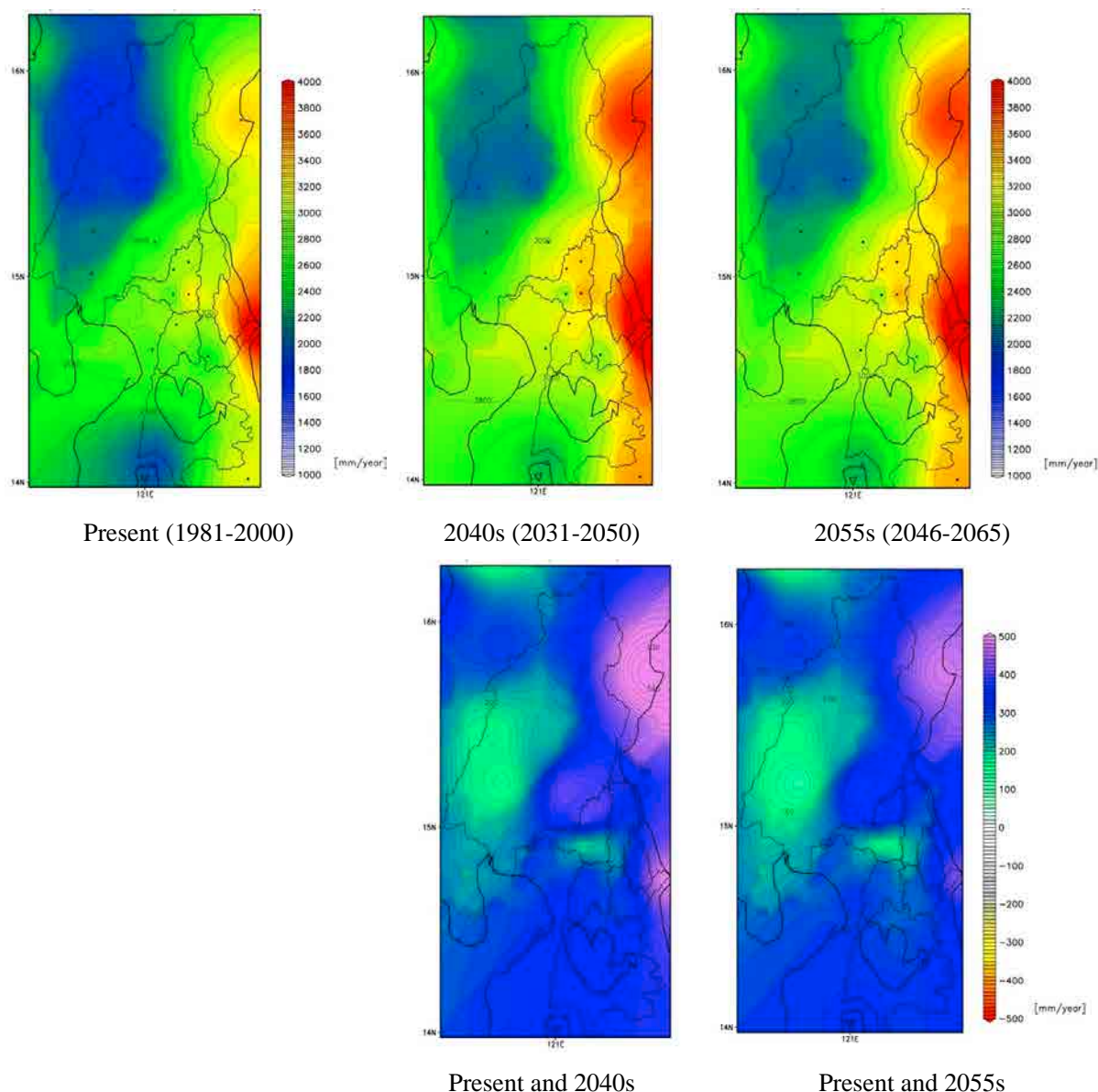
Note: The upper panel shows the ensemble mean annual rainfall for the present, 2040s, and 2055s periods. The lower panel shows the difference between their mean annual rainfall in mm/year.
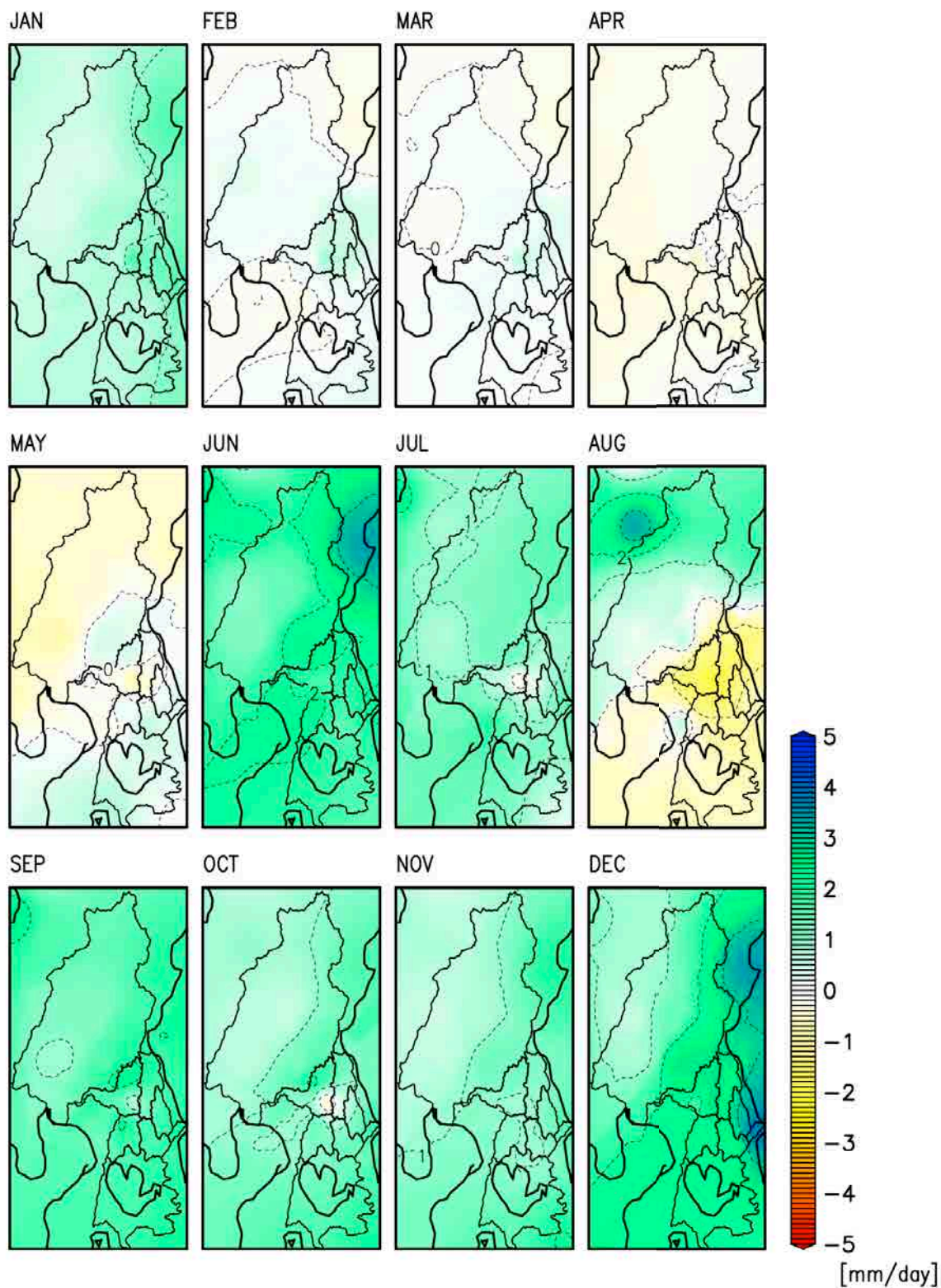
Source: JICA Study Team

Figure 8.11   Comparison Between the Ensemble Mean Annual Rainfall of the Present, 2040s, and 2055s Climate
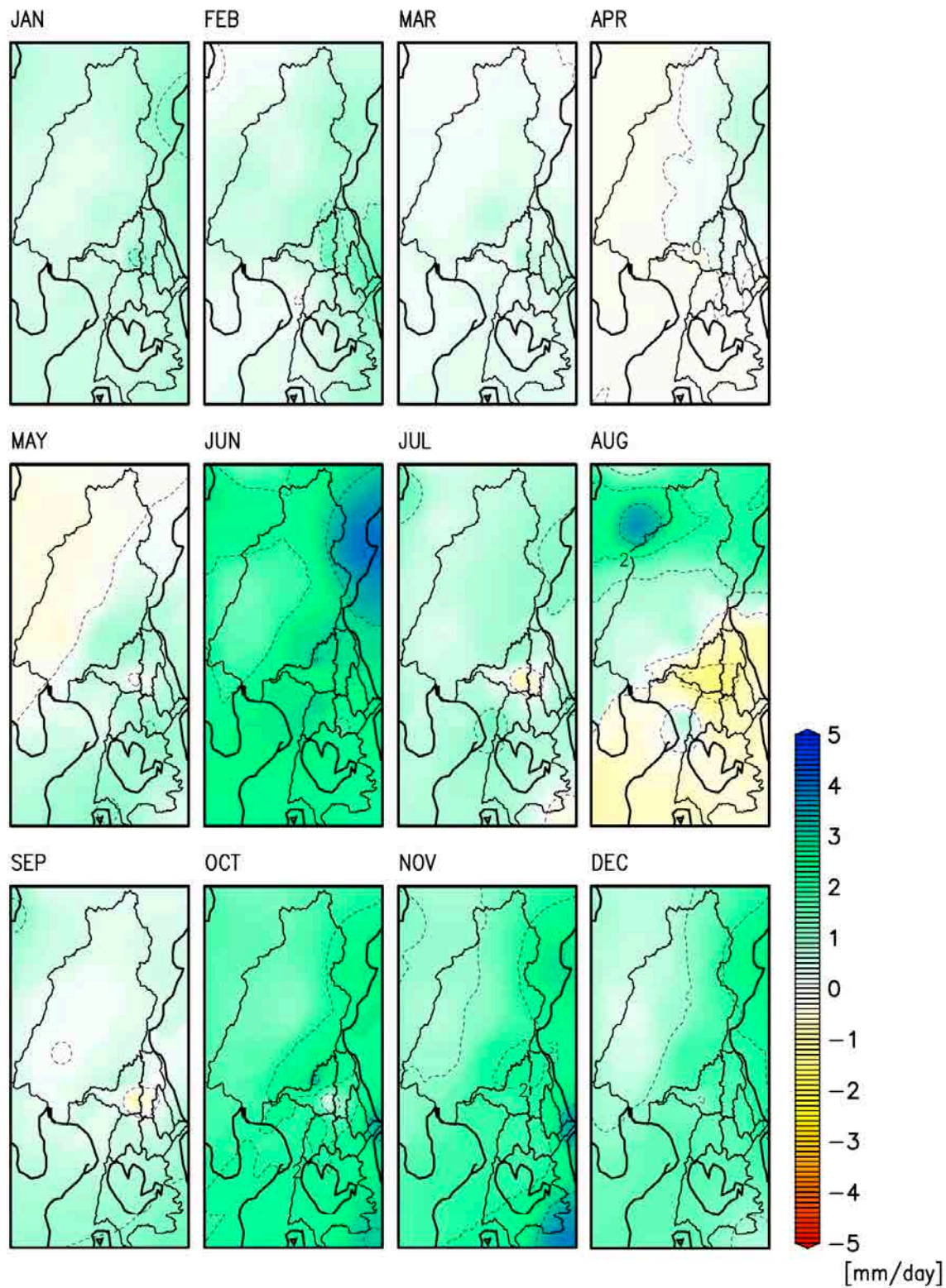
Source: JICA Study Team

Figure 8.12   Difference Between the Ensemble Mean Monthly Rainfall of 2040s and the Present Climate

Source: JICA Study Team

Figure 8.13   Difference Between the Ensemble Mean Monthly Rainfall of 2055s and the Present Climate

8.6.2   Climate Change Impact on Surface Air Temperature

The comparison of the annual mean temperatures of the present, 2040s, and 2055s are shown in Figure 8.13. The annual mean temperatures were calculated by the ensemble mean of the ten GCMs which were selected prioritizing temperature reproducibility. The 2040s data were obtained through simple projection using the ratio of the monthly mean temperature which can be obtained from the IPCC data distribution center.

The annual mean surface air temperature is expected to rise at about 1.8-1.9°C in the target year and 3.0-3.4°C in the 2055s. The difference between the annual mean temperature and the present is shown in Figure 8.14. The monthly differences are shown in Figure 8.15 for 2040s and in Figure 8.16 for 2055s. The difference between the temperatures of each month is minimal.

8.6.3   Climate Change Impact on Potential Evapotranspiration

The actual evapotranspiration was computed in the rainfall-runoff analysis. In the hydrological simulation model, the water content on the basin surface was simulated and the amount of evapotranspiration was calculated from the energy budget and vegetation distribution. The amount of evapotranspiration calculated by the runoff model was determined not only by the increase in temperature, but also by the land covers. In order to easily understand the climate change's impact on evapotranspiration, the potential evapotranspiration was calculated from the daily temperature using Harmon's equation.

Estimation of potential evapotranspiration – Harmon's Equation

$$E_t = 0.14 D_0{}^2 P_t \ [mm/day]$$

where, E_t is the daily potential evapotranspiration, D_0 is the ratio of day length to 12 hours, and P_t is the saturated vapor pressure at the daily average temperature, t [$^{\circ}$C].

Day length D[hr] can be obtained by using the following equation:

$$D = 24 - \frac{24}{\pi} \frac{\arccos\left(\sin\left(0.8333 \frac{\pi}{180} \right) + \sin\left(L \frac{\pi}{180} \right) \sin(P) \right)}{\cos\left(L \frac{\pi}{180} \cos(P) \right)} \ [hr]$$

$$P = \arcsin\left[0.39795 \cos\left(0.2163108 + 2.0 \arctan\left(0.9671396 \tan\left(0.00860 \left(J - 186 \right) \right) \right) \right) \right]$$

where, L is the latitude [deg] and J is the day of the year.

The potential evapotranspiration will increase for all over the subjected area, since the air temperature is also expected to rise in the future. The comparisons of the annual potential evapotranspiration are shown in Figure 8.17 and the monthly comparisons are illustrated in Figures 8.18 and 8.19. The increase in evapotranspiration was evaluated to be around 140 mm/yr on plain areas and around 80 mm/yr on mountainous areas for 2040s climate. The expected annual amount of evapotranspiration for the 2055s climate is double of that of the 2040s climate.

Present (1981-2000)   2040s (2031-2050)   2055s (2046-2065)

Present and 2040s   Present and 2055s
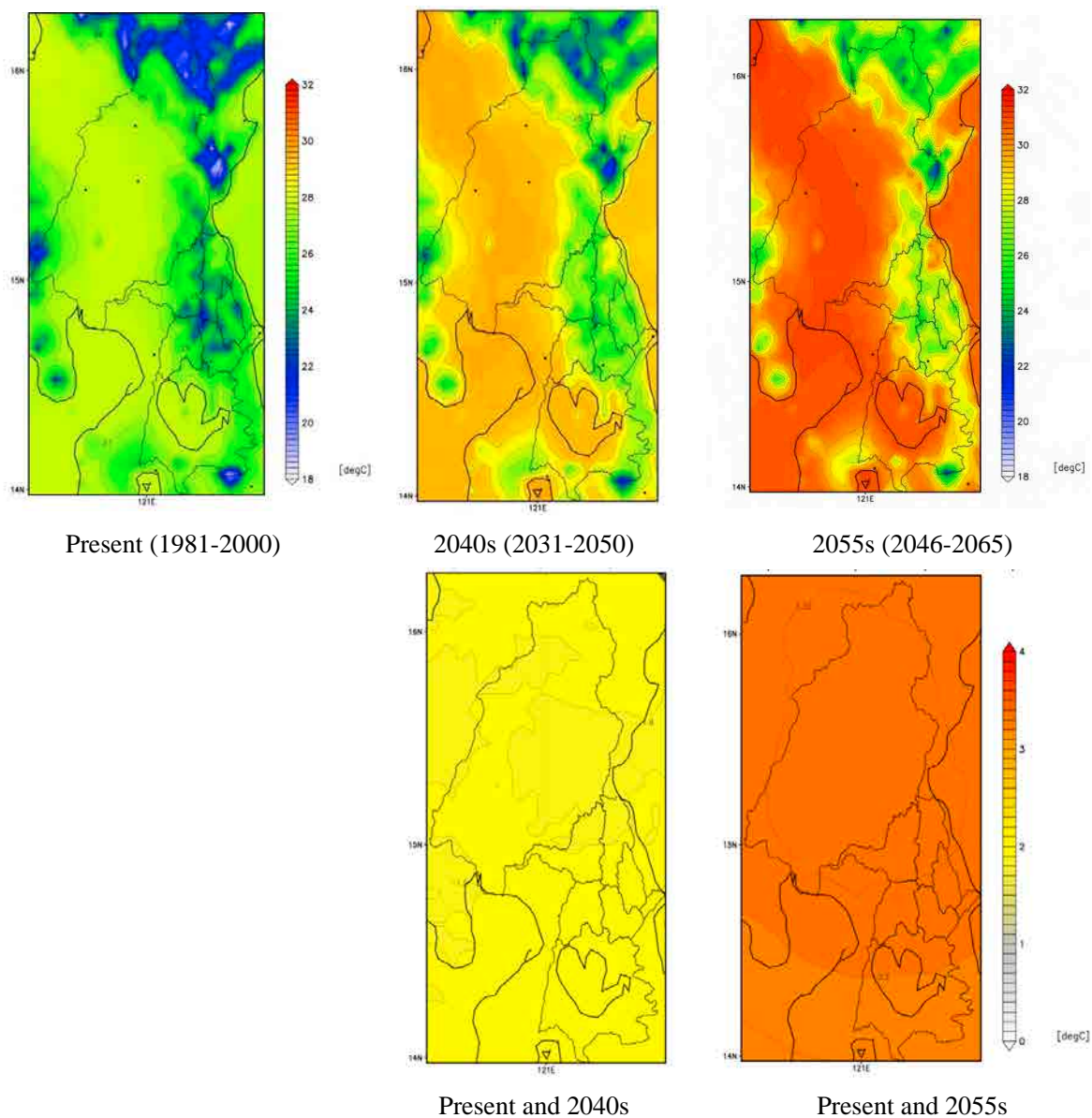
Note: The upper panel shows the ensemble mean annual surface air temperatures of the present, 2040s, and 2055s climate periods. The
        lower panel shows the differences between their mean annual surface air temperatures in °C.
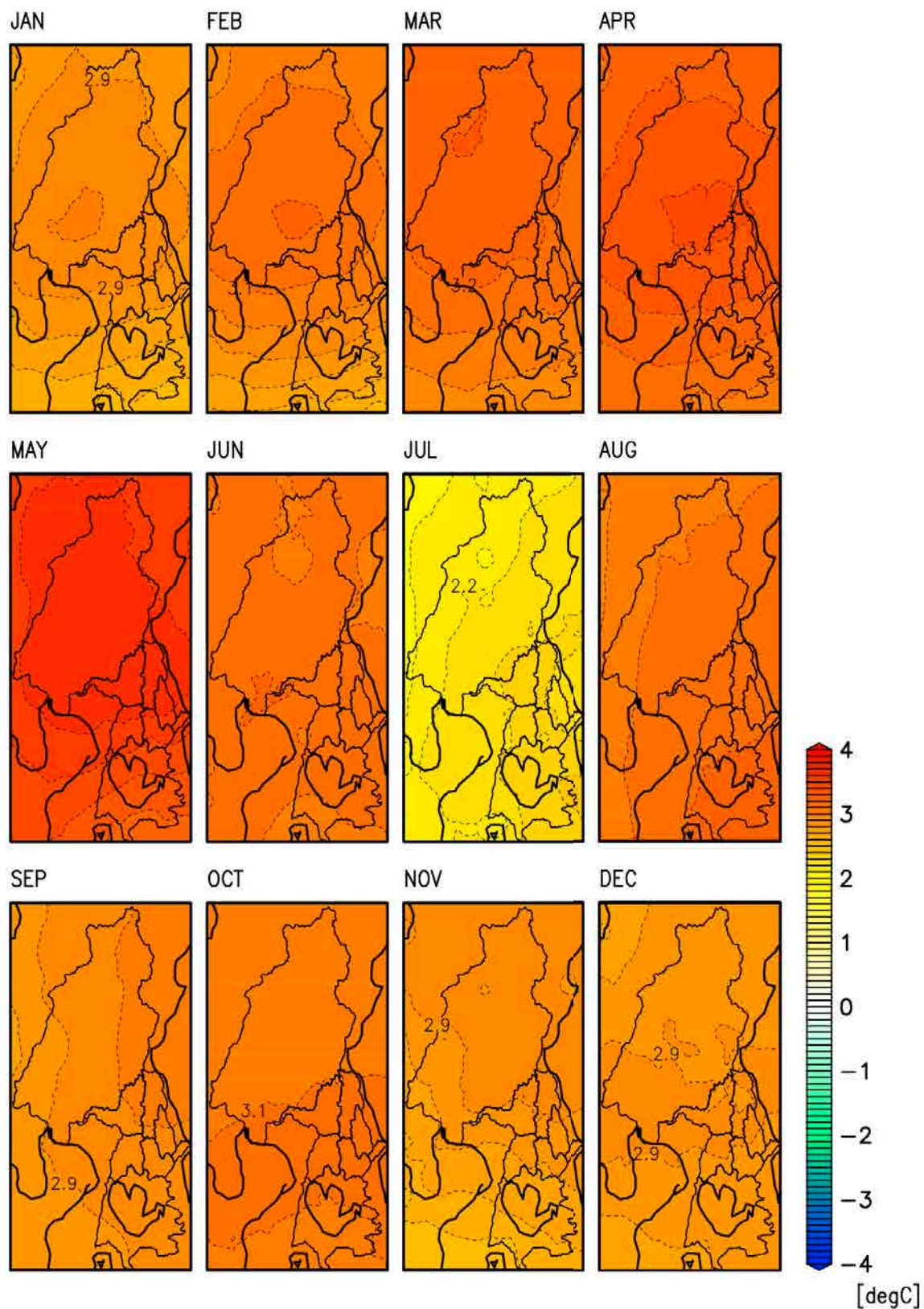Source: JICA Study Team

**Figure 8.14   Comparison Between the Ensemble Mean of Annual Mean Temperatures of the
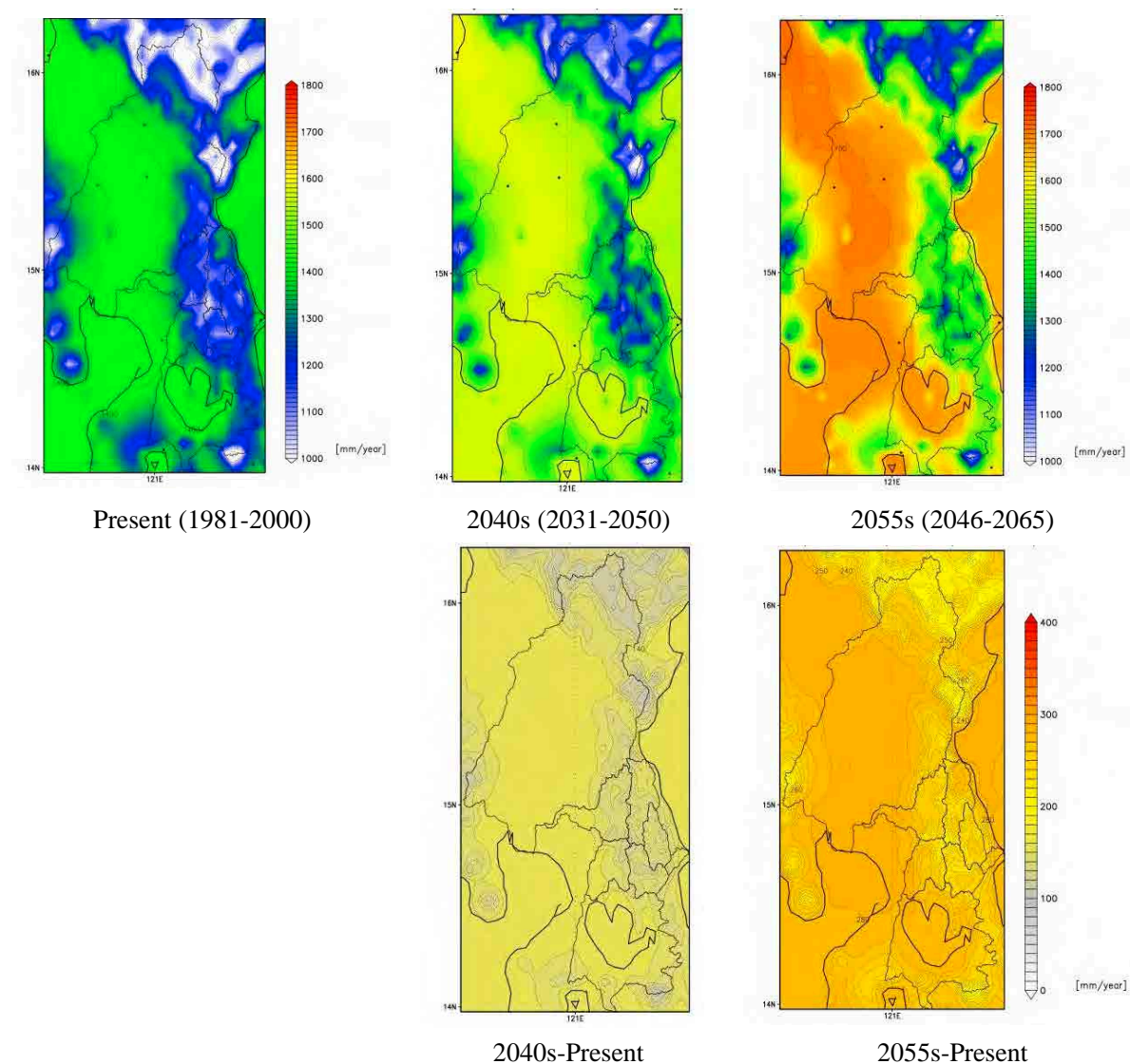   Present, 2040s, and 2055s Climate**
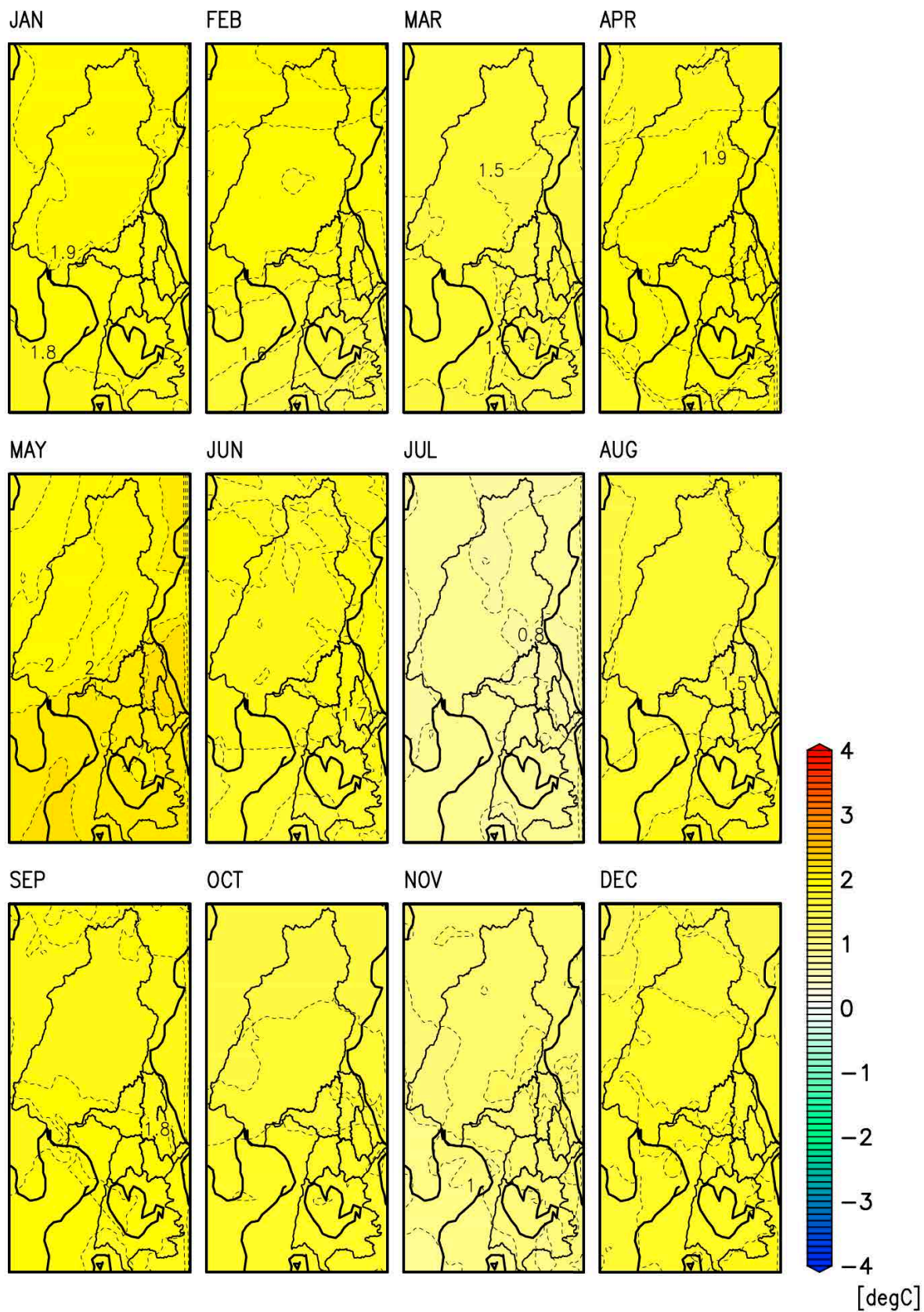
Source: JICA Study Team

Figure 8.15   Difference Between the Ensemble Mean Monthly Surface Air Temperatures of 2040s and the Present Climate

Figure 8.16   Difference Between the Ensemble Mean Monthly Surface Air Temperatures of 2055s and the Present Climate

Present (1981-2000)　　　2040s (2031-2050)　　　2055s (2046-2065)

2040s-Present　　　2055s-Present

Note:　The upper panel shows the ensemble mean annual evapotranspiration of the present, 2040s, and 2055s climate periods. The lower panel shows differences of their mean annual evapotranspiration in mm/year.
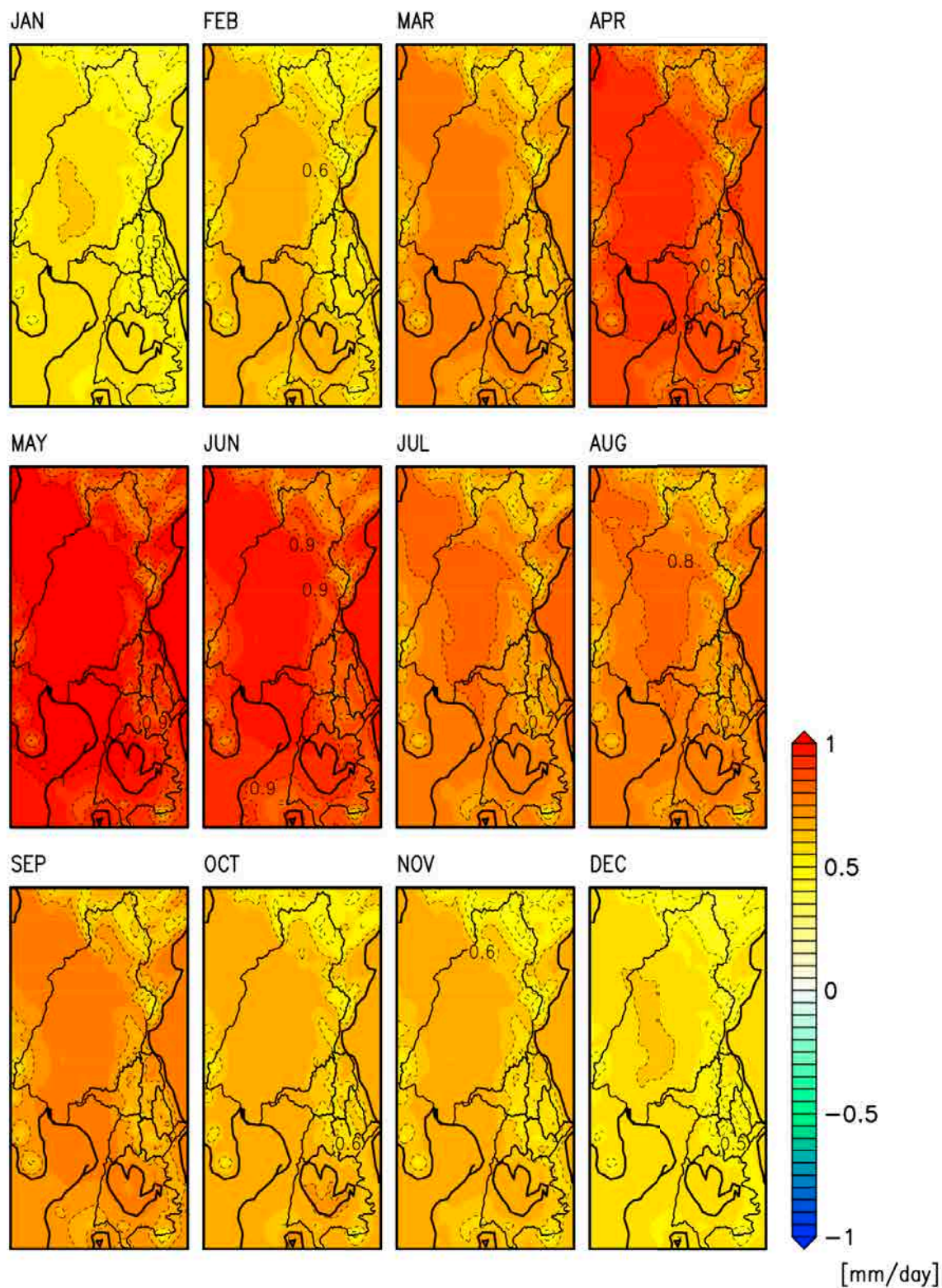
Source: JICA Study Team

Figure 8.17　Comparison of the Ensemble Mean Annual Evapotranspiration of the Present, 2040s, and 2055s Climate
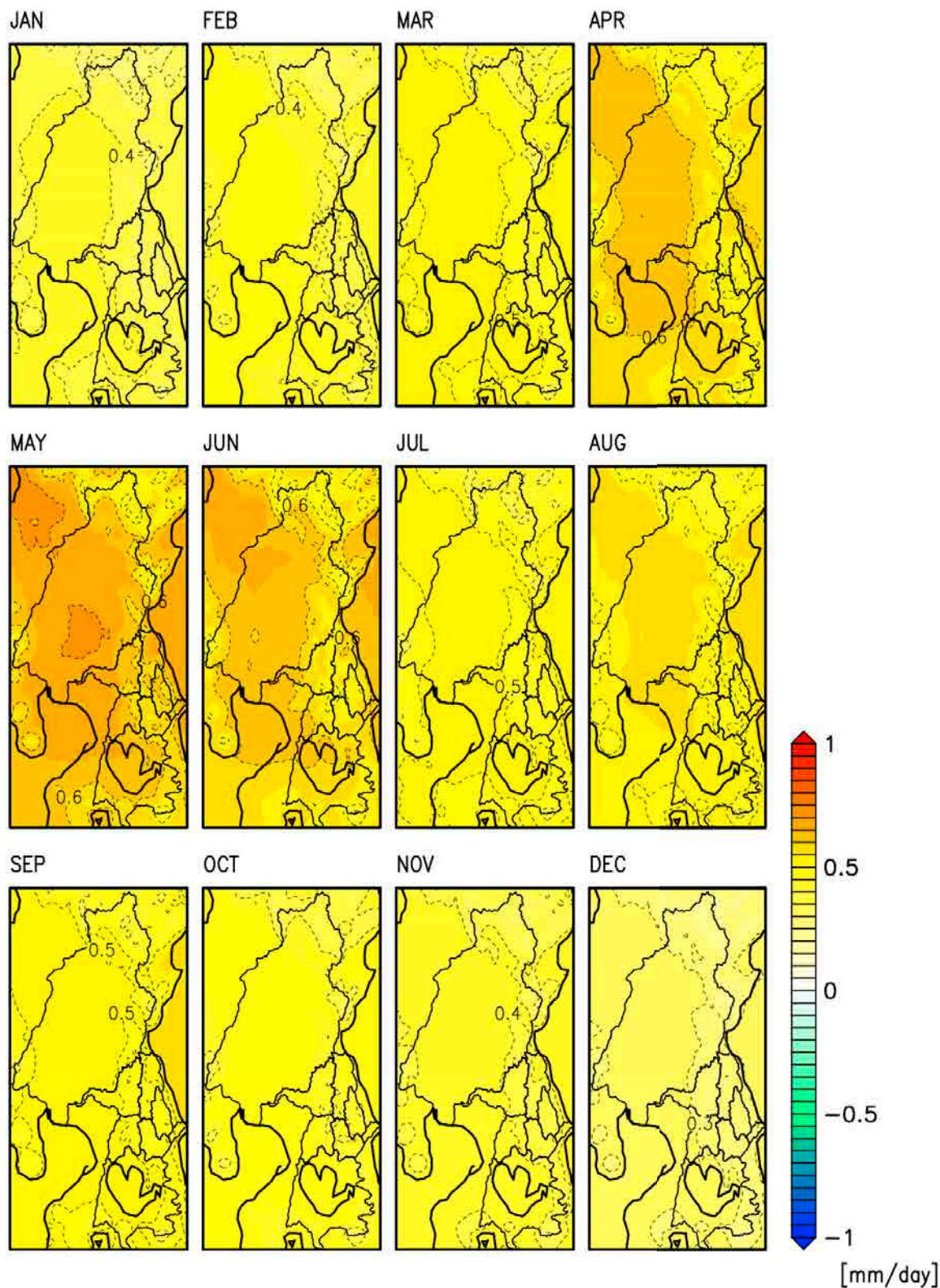
Source: JICA Study Team

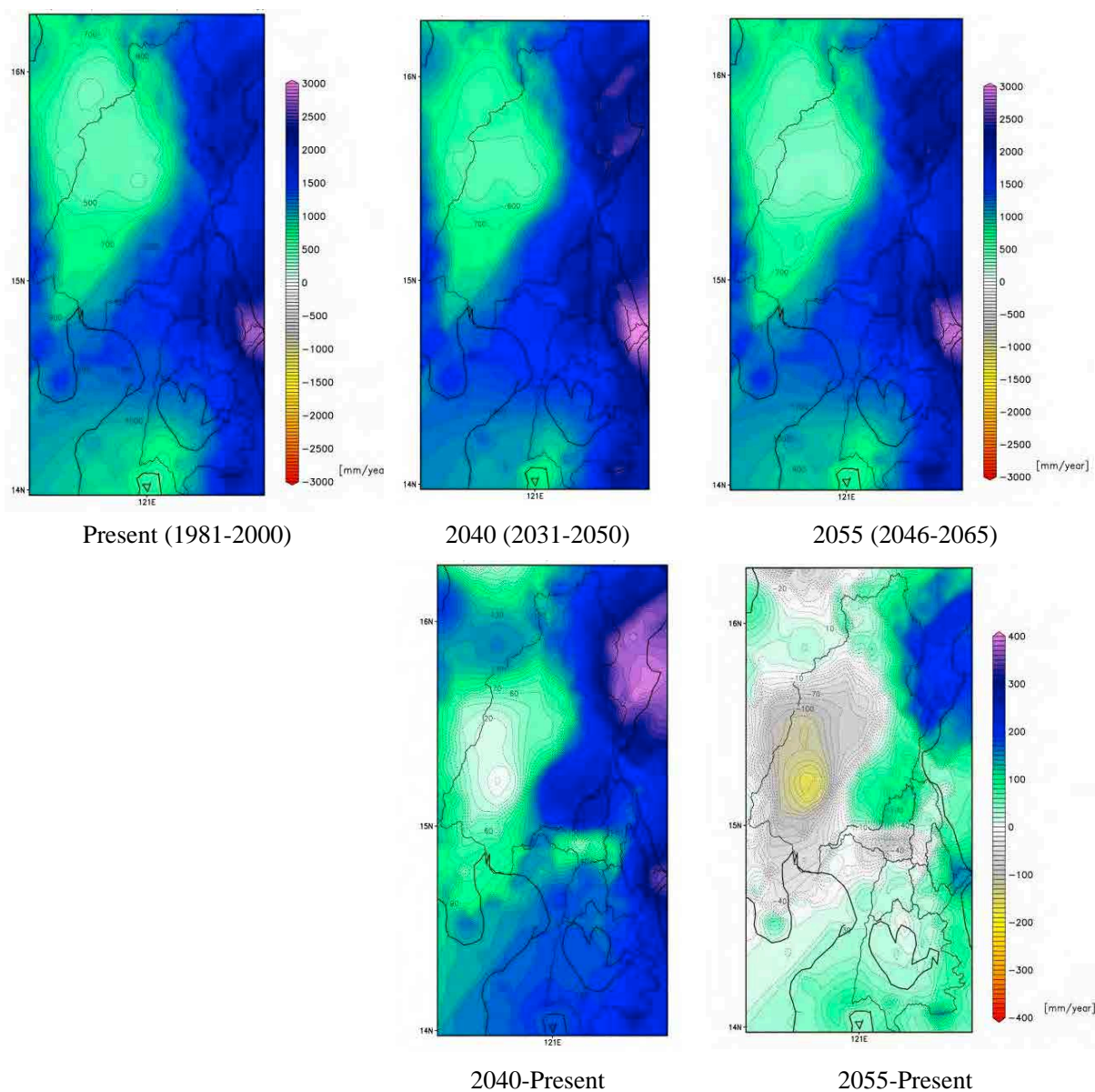**Figure 8.18   Difference Between the Ensemble Mean Monthly Evapotranspiration of 2040s and the Present Climate**

Source: JICA Study Team

Figure 8.19   Difference Between the Ensemble Mean Monthly Evapotranspiration of 2055s and the Present Climate

8.6.4   Climate Change Impact on P-E

The precipitation minus the potential evapotranspiration, or P-E, can be considered as the summary of the climate change impact on the water resources. The comparison of the annual P-E of the present, 2040s, and 2055s climate periods are shown in Figure 8.20. The differences between the future monthly P-E and present P-E are shown in Figures 8.21 and 8.22.

The annual P-E in the 2040s is expected to increase considering the present values. The increase on the western part of the Pampanga River basin is very low or almost the same as the present condition. In 2055s, most parts of the Pampanga River basin will suffer from the drier pressure due to climate change. It is important to note that these were evaluated using the potential evapotranspiration. The effect of the actual evapotranspiration will be calculated considering the rainfall-runoff model which is discussed in the next chapter.

Present (1981-2000)

2040 (2031-2050)

2055 (2046-2065)

2040-Present

2055-Present

None: The upper panel shows the ensemble mean P-E of the present, 2040s, and 2055s climate periods. The lower panel shows differences of their mean P-E in mm/year.

Source: JICA Study Team

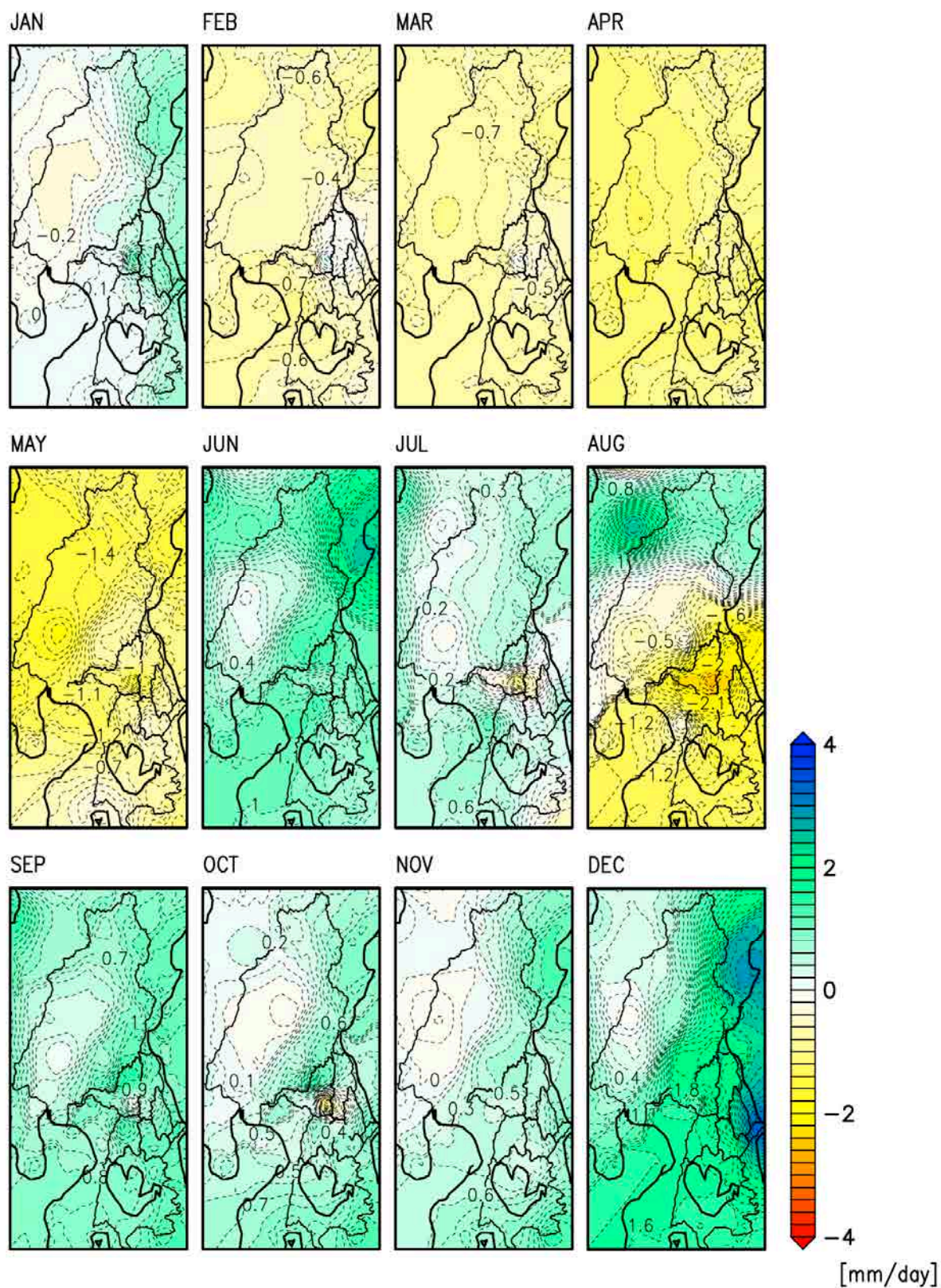**Figure 8.20   Comparison Between the Ensemble Mean Annual Precipitation Minus the Potential Evapotranspiration of the Present, 2040s, and 2055s Climate**
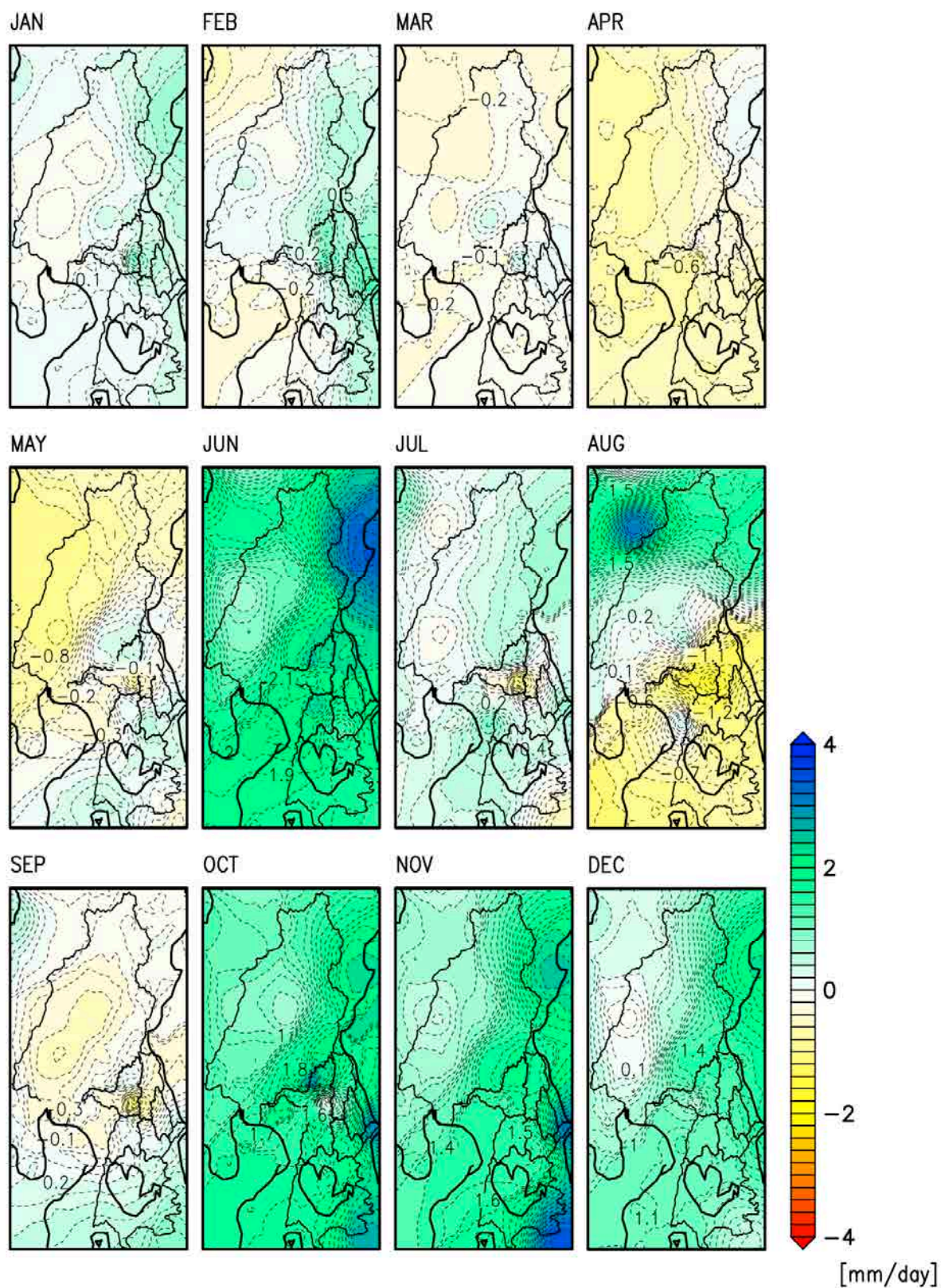
Source: JICA Study Team

Figure 8.21   Difference Between the Ensemble Mean Monthly P-E of and the Present Climate

Source: JICA Study Team

Figure 8.22   Difference between the Ensemble Mean Monthly P-E of 2055s and the Present Climate

8.6.5 Climate Change Impacts on Subject Basins

The basin averages of the evaluated meteorological variables, namely, precipitation, air temperature, potential evapotranspiration, and P–E were calculated for the target basins. The results of evaluating the climatology of monthly values are shown in Figures 8.23 to 8.26. The future lines in the charts are the ensemble means of the selected GCMs, where six were selected for the evaluation of precipitation, and ten were selected for the evaluation of air temperature and evapotranspiration.

(1) Precipitation

The seasonal precipitation patterns for each basin were reproduced by bias correction. The future change in seasonal rainfall patterns is expected to be minimal and the seasonal patterns of the future trace the trend of the present. The amount of monthly rainfall will increase in the future especially for the rainy season, from May to November.

There are no expected significant differences on the changing pattern in the future for the six subjected basins. This might be caused by the limitation evaluation using GCMs, because the grid sizes of GCMs are large as compared with the subjected basin scale. Some GCMs covers the whole Study Area with a single grid. The seasonal pattern and increasing trend can be evaluated by bias correction of GCMs, but it might be difficult to know the differences among the basins, although the methodology of evaluation and the GCMs themselves are among the most advanced techniques in the world at present.

(2) Surface Air Temperature

The rise in the amount of air temperature for every subjected basin will be 1.5-1.8 ^{o}C towards 2040s and 3.0 ^{o}C towards 2055s. The temperature will rise evenly through the years. In the future, the expected differences in the change in air temperature among the basins are minimal.

(3) Potential Evapotranspiration

The potential evapotranspiration changes as air temperature changes, since the potential evapotranspiration was derived from the daily air temperature. The increasing rates of evapotranspiration in the subjected basins toward 2040s are evaluated to be about 0.2-0.5 mm/day, and those toward 2055s are to be about 0.8-1.0 mm/day.

(4) P–E (Precipitation minus Potential Evapotranspiration)

The P–E can be considered as the index of the climate change impact on the external forces of hydrological condition. There are negative values of P-E for dry seasons, from January to April. It is important to note that the negative values will be enhanced towards the future and the increasing negative value will be small. The period covered by the negative P-E of the Agos River basin is only two months (March and April). Meanwhile, for the other basins, the period covered is four months (January to April). The pressure of drought in the Agos River basin is lighter among the other basins.

The P–E during the rainy season is expected to increase. This will lighten up the conditions of water resources. Figures 8.23 to 8.26 shows the impact of climate change on the average precipitation, air temperature, potential evaporation, and P-E of the target basins.
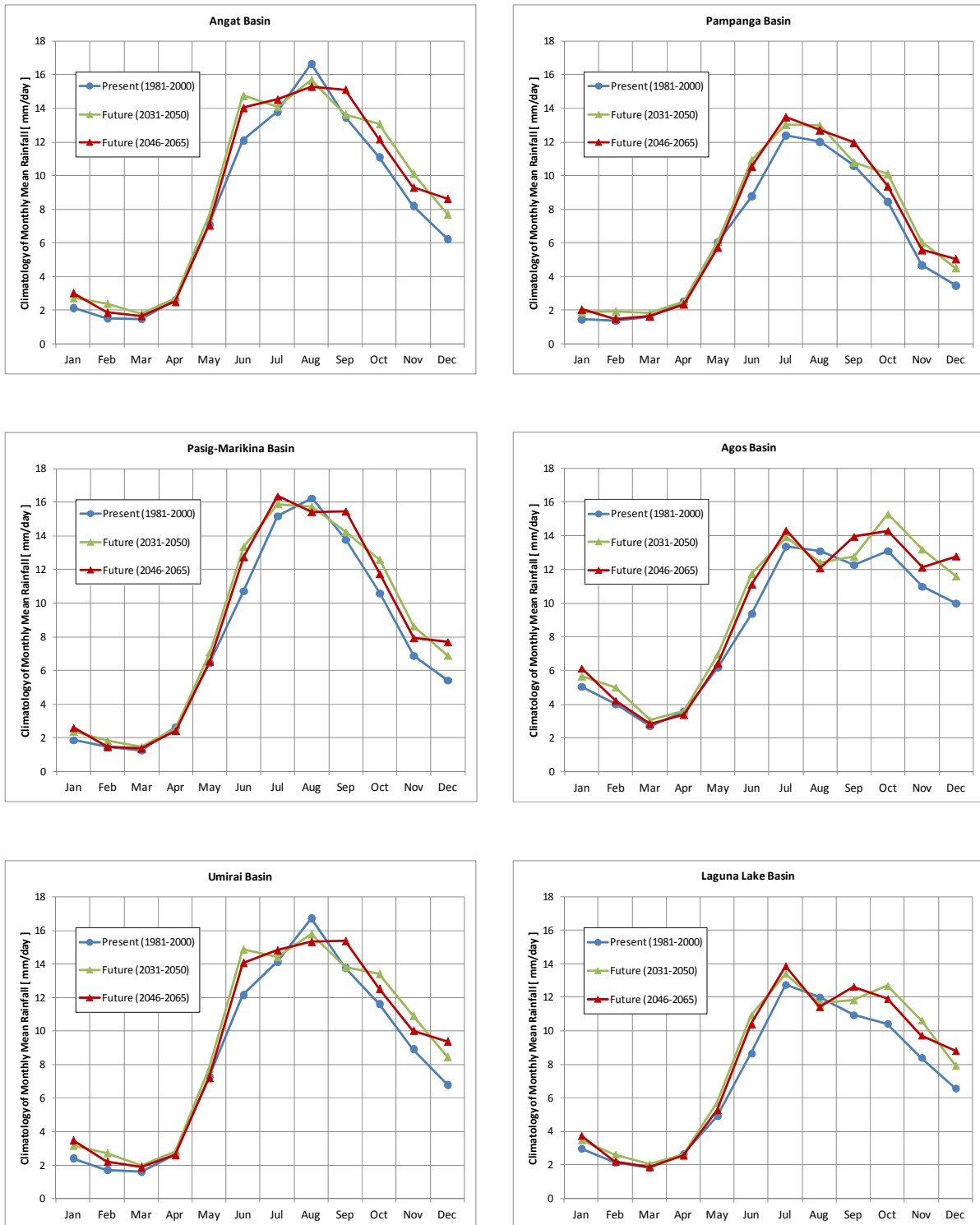
Source: JICA Study Team

Figure 8.23   Impact of Climate Change on the Climatology of the Average Precipitation of the Subjected Basins
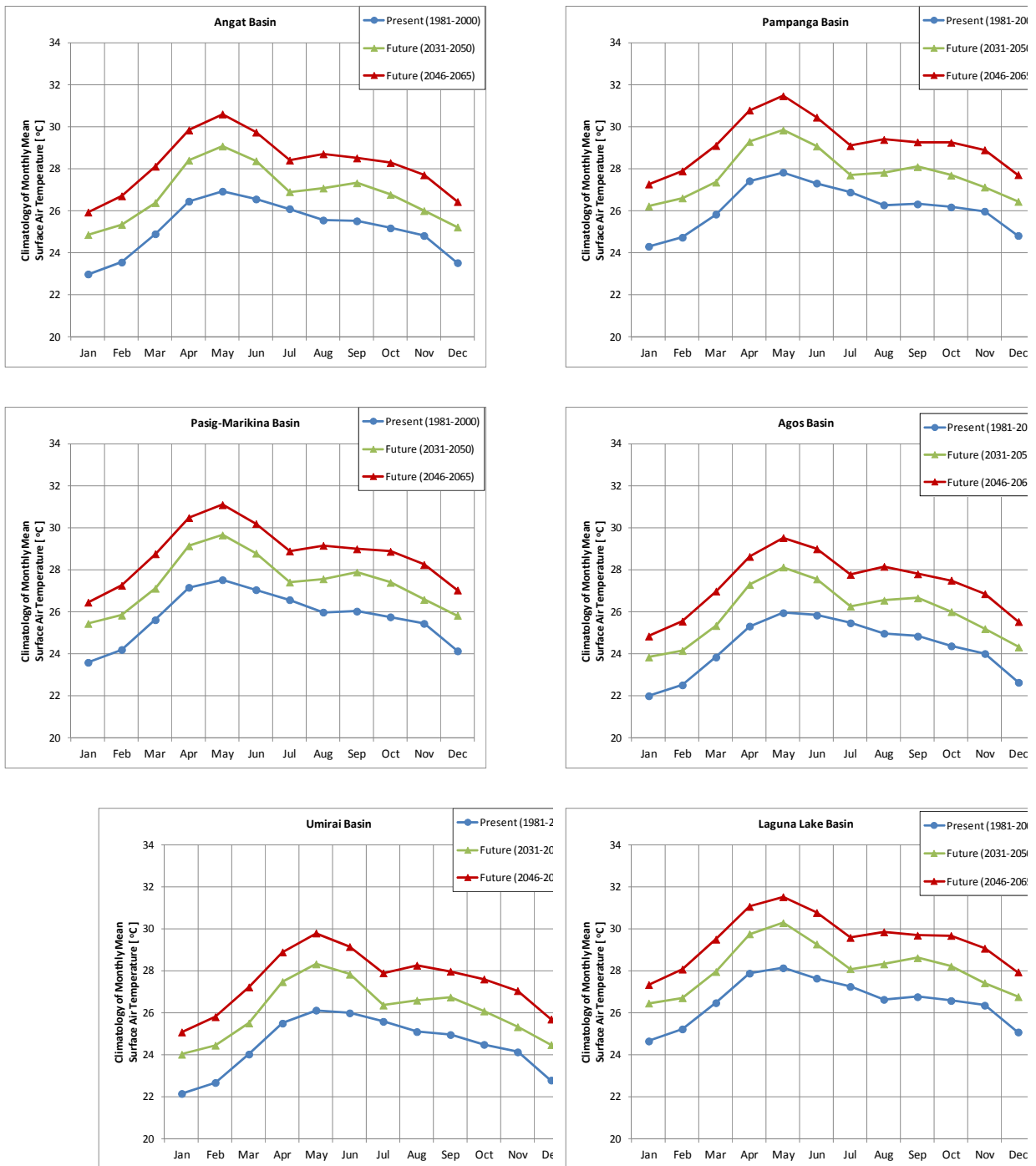
Source: JICA Study Team

Figure 8.24   Impact of Climate Change on the Climatology of the Average Air Temperature of the Subjected Basins

Source: JICA Study Team

Figure 8.25   Impact of Climate Change on the Climatology of the Average Potential
Evapotranspiration of the Subjected Basins
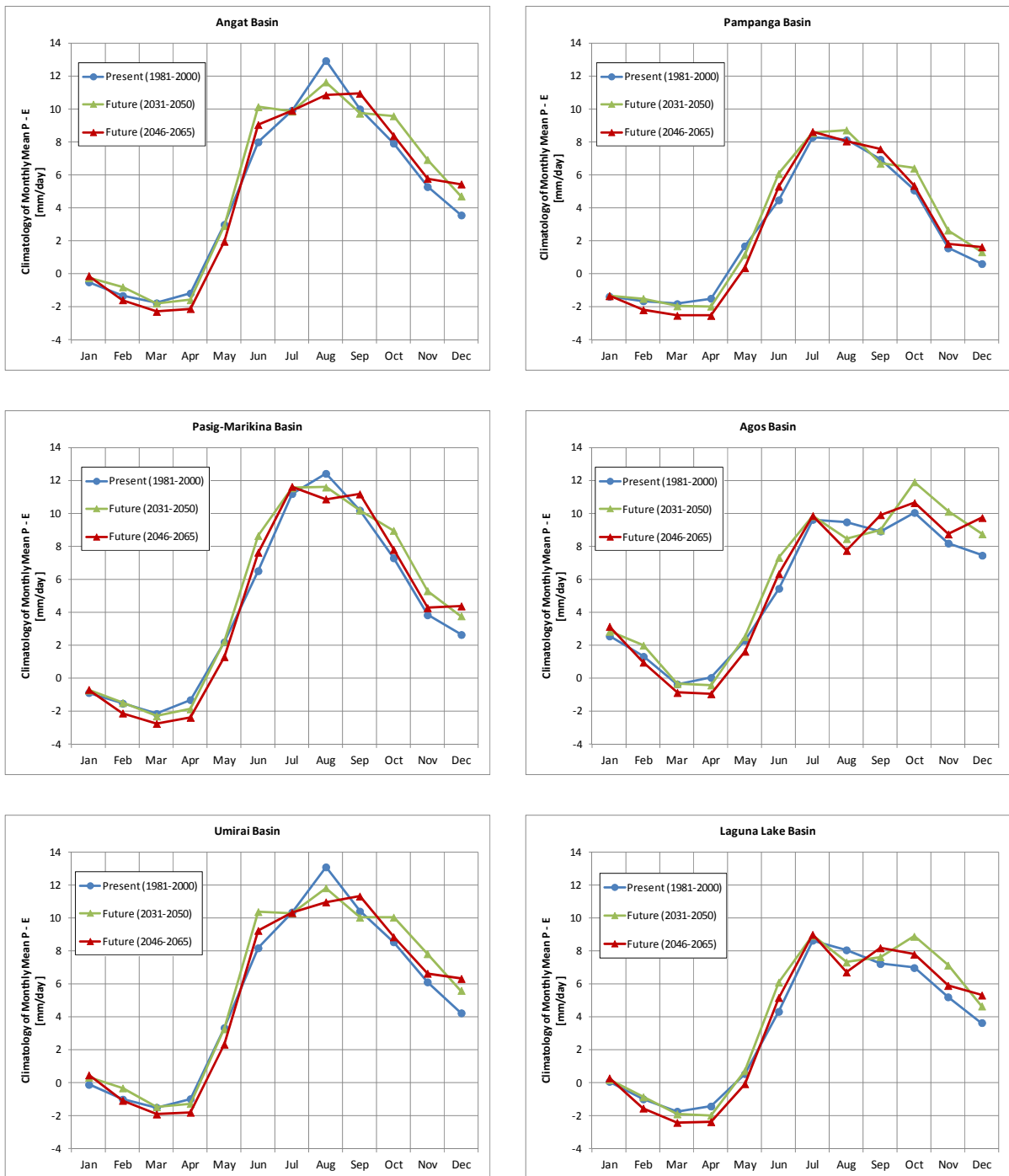
Source: JICA Study Team

**Figure 8.26   Impact of Climate Change on the Climatology of the Average Difference of
Precipitation minus Potential Evapotranspiration of the Subjected Basins**

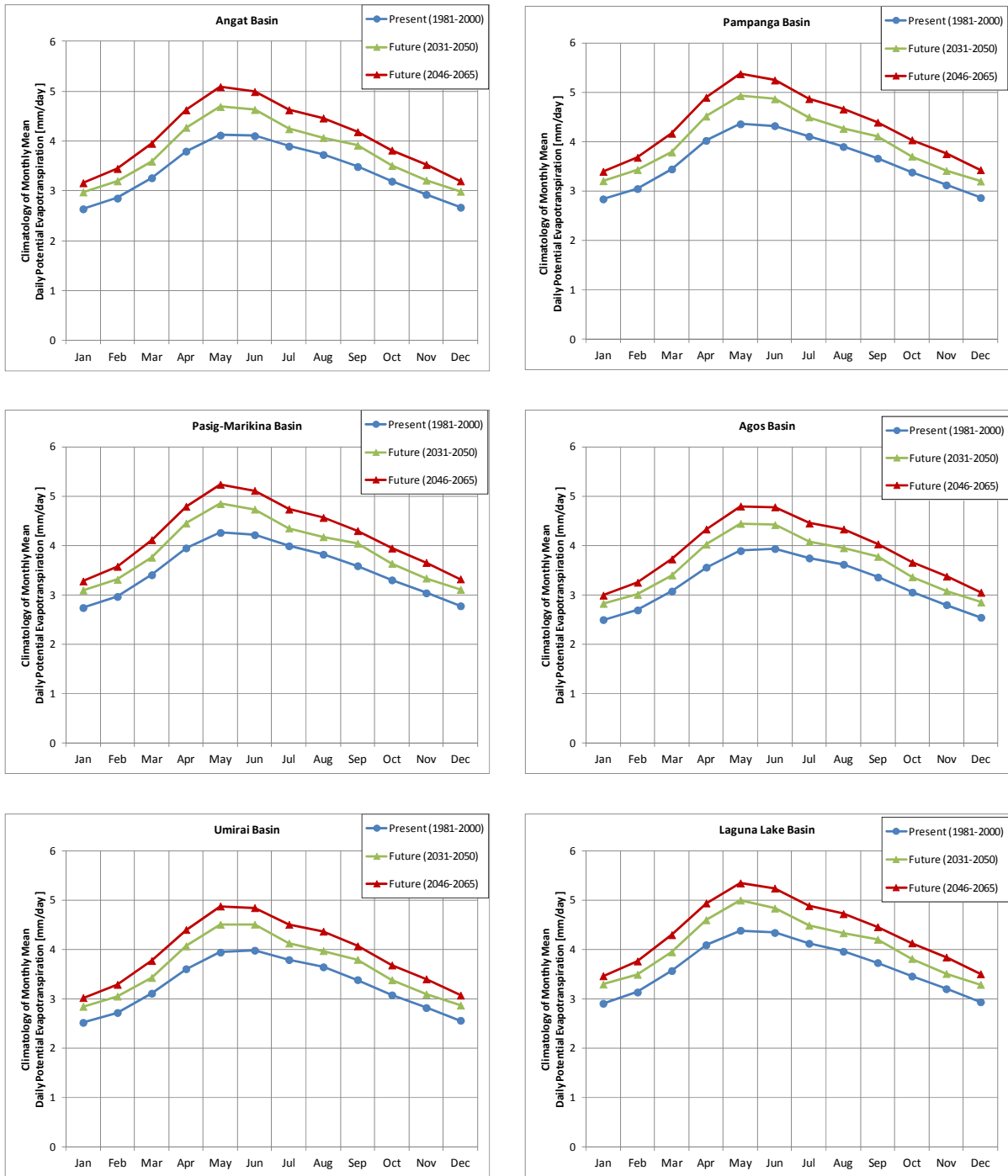# CHAPTER 9   RUNOFF ANALYSIS AND THE IMPACTS OF CLIMATE CHANGE OVER THE WATER RESOURCES

9.1   Rainfall Runoff Model

Two types of physical based runoff models, namely, the Water and Energy Budget-based Distributed Hydrological Model (WEB-DHM) and Similar Elements of Hydrological Response (SHER) Model were applied in the Study. The runoff model for evaluating the impact of the climate change on the hydrological condition must be able to evaluate the effects of changes in seasonal patterns of rainfall and temperature on the river flow, groundwater level and evapotranspiration.

WEB-DHM, which can simulate very detailed energy budget, was applied for the evaluation of all target basins except the Laguna Lake basin. The Laguna Lake basin is a very flat area consists of a number of small catchments, and these conditions made it difficult to build a topological process for the lake basin using the WEB-DHM. The SHER model, which is a physical-based distributed model, was applied for the evaluation of hydrological conditions for the Laguna Lake basin. SHER model does not have a detailed model for evaluation of evapotranspiration compared with WEB-DHM. However, the SHER model can be applied to flat areas and complicated catchment systems.

9.1.1   WEB-DHM

As a distributed biosphere hydrological model, the WEB-DHM has been developed by fully coupling a biosphere scheme (SiB2) with a geomorphology-based hydrological model (GBHM). SiB2 describes the transfer of turbulent fluxes, such as energy, water, and carbon fluxes, between the atmosphere and land surface for each model grid. The GBHM redistributes water moisture laterally through the simulation of both surface and subsurface runoff using grid-hillslope discretization, and then to flow routing in the river network.

The model structure of the WEB-DHM is shown in Figure 9.1.
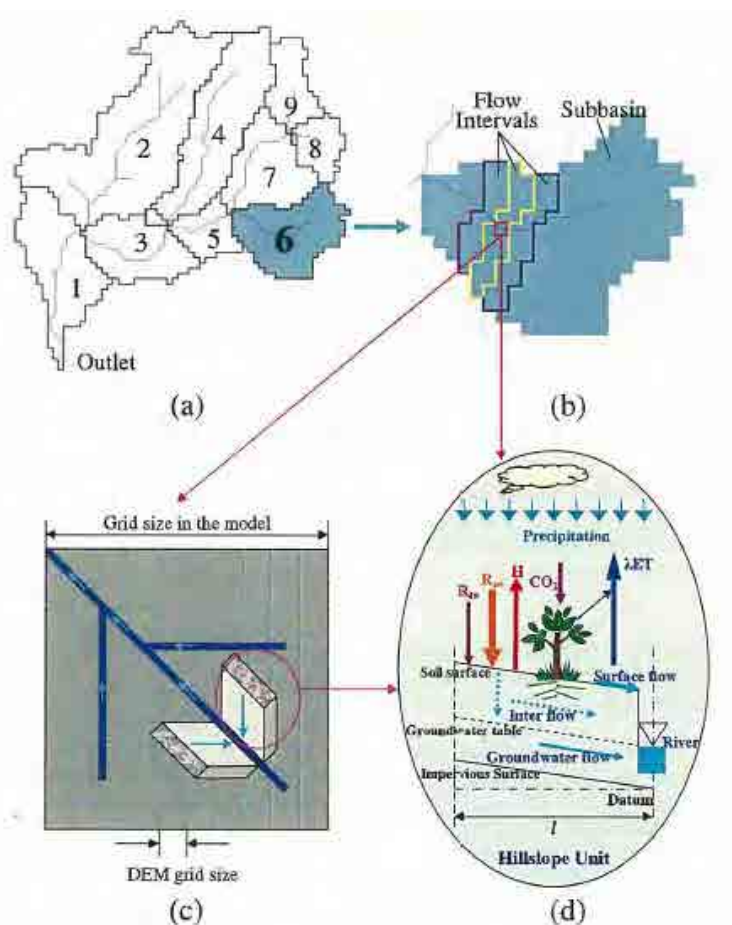
Source: University of Tokyo

Figure 9.1   Overall Structure of the WEB-DHM

(a) Division from a basin to sub-basins, (b) subdivision from a sub-basin to flow intervals comprising several model grids, (c) discretization from a model grid to a number of geometrically symmetrical hillslopes, and (d) process descriptions of water moisture transfer from the atmosphere to the river.

9.1.2   SHER Model

The detailed modeling for the Laguna Lake was difficult because the sea water from Manila Bay and the fresh water of the lake are exchanging depending on the tidal variation. It can be conceived that the annual water budget of sea water is balanced to zero. The runoff analysis for the tributaries surrounding the Laguna Lake will be conducted.

The SHER model will be applied for the tributaries. The SHER model was developed by Dr Mushiake, a professor emeritus of the University of Tokyo, and Dr Srikantha Herath, a professor of the United Nations University. The SHER model is also a physically-based model but the elements are not grid-based but are according to the arbitrary form of the sub-basin. The parameters within a sub-basin of the SHER model are not distributed. Therefore, the delineation of the surface and ground water block is a key point in order to achieve accurate runoff analysis. The SHER model does not have an energy budget component, unlike the WEB-DHM. The evapotranspiration is evaluated by simulating the water content in sub-surface soil with the potential evapotranspiration data, which is one of the input data for the SHER model. Figure 9.2 shows the scheme in using the SHER model.
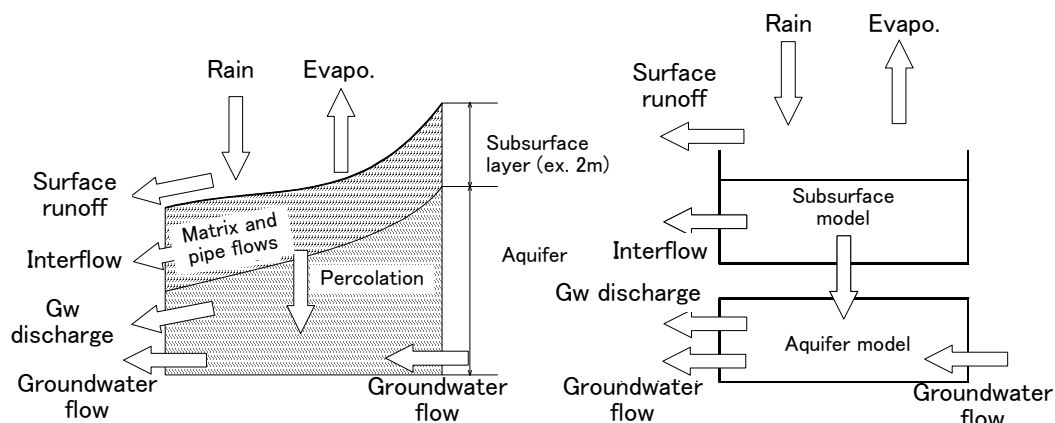
Source: JICA Study Team

Figure 9.2   Schematic Image of SHER Model

9.2   Input Data for Runoff Model

9.2.1   Soil Parameters

The 1975 USDA soil classification was used for the local soil taxonomy. This has been converted to the Food and Agriculture Organization (FAO) classifications by overlaying the FAO soil map on the local map, as shown in Table 9.1. Soil parameters were based on the intrinsic properties of each soil type taken from the FAO global dataset. Figure 9.3 shows the distribution of soil types as defined by the classifications of FAO.

Table 9.1   Soil Classification

USDA 1975; Local Soil Classification	Soil Class (FAO)	FAO Number
Laguna de Bay and Taal Lake	Water	0
Tropudults w/Tropudalfs Tropepts & Oxisols	Nitosol	4413
Mountain soil with entisol, inceptisol, and ultisol; and alfisol with thermic, hyperthermic, and isothermic temperature regimes	Acrisol	4465
Entropepts with dystropepts	Cambisol	4478
Tropaquepts with hydraquents	Gleysol	4503
Tropudalfs with tropepts	Gleysol	4504
Pellusterts with udalfs, udorthents, and tropepts; and tropquepts with entropepts	Luvisol	4537
Contested Area	Nitosol	4546
Tropopsamments with troporthents	Arenosol	4564
Chromusterts with udalfs, udorthents, and tropepts	Vertisol	4582
Eutrandepts with eutropepts	Vertisol	4589

Source: JICA Study Team, based on DENR and FAO datasets
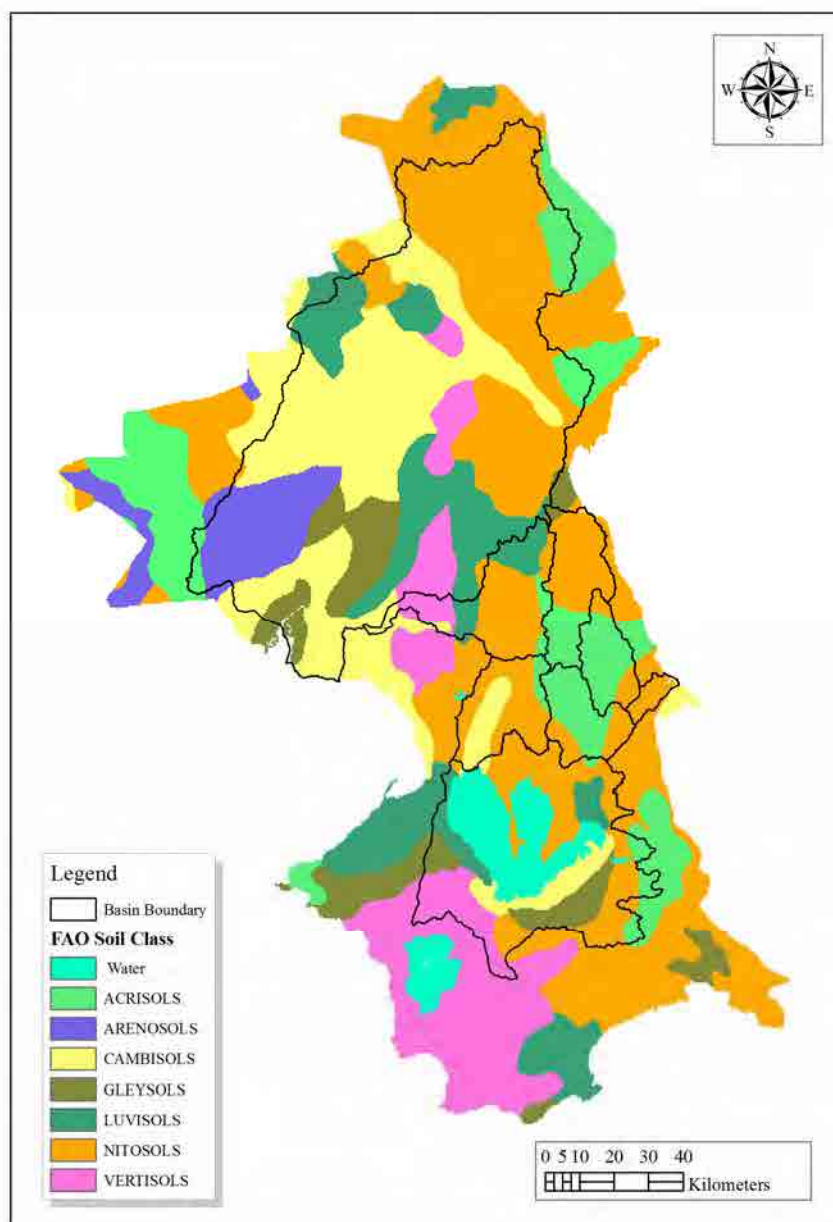
Source: JICA Study Team with the Department of Environment and Natural Resources and FAO datasets
Figure 9.3   Distribution of Soil Types Defined by FAO

9.2.2   Vegetation Parameters

Local land use has been classified under SiB2 by overlaying the SiB2 land use map on the local map. Table 9.2 shows the land use and vegetation classification while Figure 9.4 shows the distribution using SiB2 classifications.

Table 9.2   Land Use and Vegetation Classification

Local Land Use Classification	SiB2 Reclassification
--	1-Broadleaf evergreen trees
Closed forest, broadleaved Open forest, broadleaved Mangrove forest	2-Broadleaf deciduous trees
Open forest, mixed Closed forest, mixed	3-Broadleaf and needleleaf trees
Closed forest, coniferous Bamboo formation	4-Needleleaf evergreen trees
	5-Needleleaf deciduous trees
Natural, grassland	6-Short vegetation/C4 grassland
Built up area Natural, barren land Woodland, fallow	7-Shrubs with bare soil
Wood land, shrubs	8-Dwarf trees and shrubs
Cultivated, annual crop Wooded land, wooded grassland Cultivated perennial crop	9-Agriculture or C3 grasslands
Fishpond Inland water	10-Water and wetlands
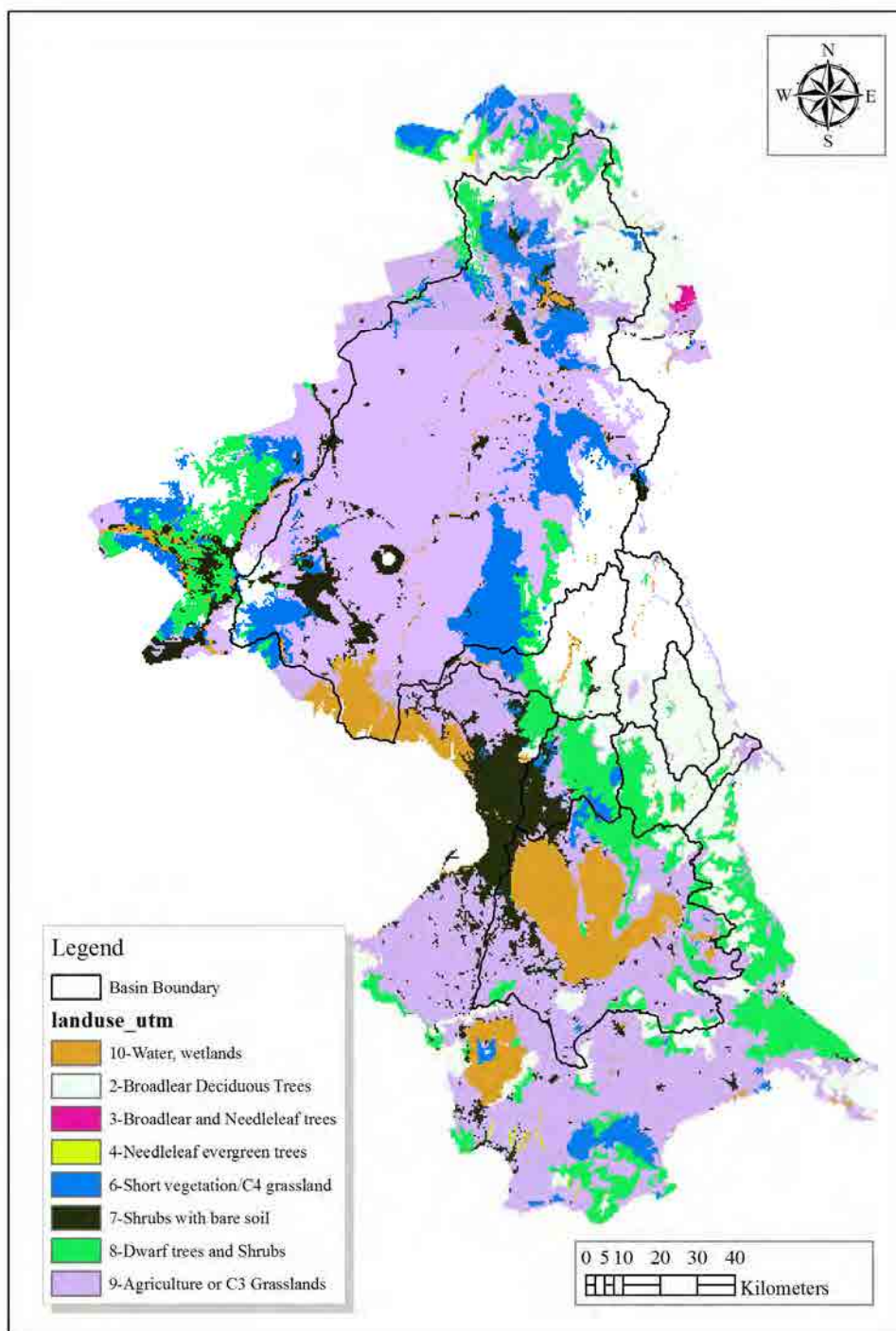
Source: JICA Study Team, based on DENR dataset

Figure 9.4   Distribution of Land Use and Vegetation Types using SiB2 Classification

9.2.3   LAI and FPAR

The leaf area index (LAI), which is an important structural property of plant canopy, is defined as one-sided green leaf area per unit ground surface area. LAI is the ratio of total upper leaf surface of vegetation divided by the surface area of the land on which the vegetation grows. LAI is a dimensionless value, typically ranging from 0 (for bare ground) to 6 (for a dense forest).

Fraction of Photosynthetically Active Radiation (FPAR) measures the proportion of available radiation in the photosynthetically active wavelengths (400 mm to 700 mm) that a canopy absorbs. LAI and FPAR are biophysical variables which describe canopy structure and are related to functional process rates of energy and mass exchange. LAI and FPAR can be derived from satellite data such as Moderate Resolution Imaging Spectroradiometer (MODIS) and Advanced Very High Resolution Radiometer (AVHRR), which are provided by the National Aeronautics and Space Administration (NASA).

9.2.4 Atmospheric Forcing Data

(1) Rainfall

Temporal Downscaling of the Observed Rainfall Data:

Basically, the collected rainfall data are all daily rainfall. For the runoff model, the rainfall data is preferable. In the tropical area, there is a significant periodical rainfall cycle in a day, but the rainfall amount caused by the diurnal cycle is not large. The diurnal cycles for the daily rainfall are studied using the hourly rainfall record in the Pampanga River basin. The rainfall gauging stations which are shown in Table 9.3 were utilized for the development of the diurnal cycle of rainfall, and available data cover from August 1973 to December 2005.

Table 9.3   Rain Gauging Stations Which Were Utilized for the Development of Diurnal Cycle

Station Name	Latitude	Longitude
Muñoz	15°44'44.4"N	120°56'34.2"E
Sapang Buho	15°35'40"N	121°04'00.5"E
Mayapyap	15°31'00"N	120°57'15.1"E
Gabaldon	15°29'55"N	121°20'21.2"E
Zaragoza	15°26'39.4"N	120°45'01.9"E
Papaya	15°21'47.8"N	121°03'55.2"E
San Isidro	15°18'49.7"N	120°54'03.2"E
Arayat	15°10'05.5"N	120°46'55.6"E
Candaba	15°06'57.8"N	120°51'09.3"E
Sibul Spring	15°10'04.8"N	121°03'32.5"E
Sasmuan	14°56'16.7"N	120°37'17.9"E
Sulipan	14°56'26.8"N	120°45'34"E
Ipo Dam	14°52'31.1"N	121°08'44.8"E
San Rafael	14°58'53.8"N	120°55'38"E

Source: JICA Study Team, based on the list of rain gauging stations of PAGASA

The diurnal cycles for daily rainfall intensities 0-50 mm/day, 50-100 mm/day, 100-250 mm/day, and above 250 mm/day were developed and graphed in Figure 9.5.
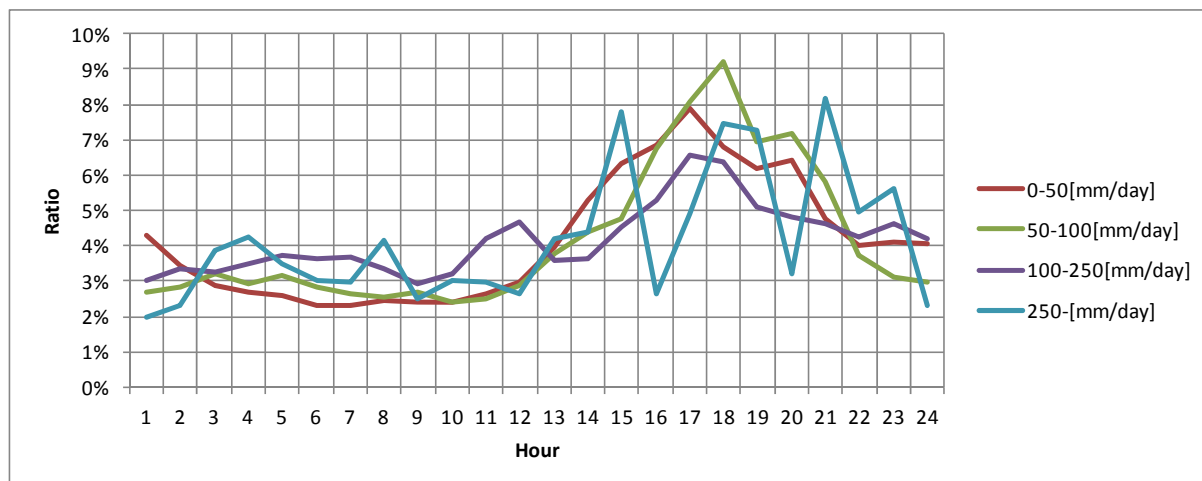
Source: JICA Study Team, based on hourly rainfall record in the Pampanga River basin

Figure 9.5   Diurnal Variation of Rainfall

Spatial Downscaling of the Rainfall:

The WEB-DHM is a grid-based distributed model and can reflect the distribution of the rainfall from the discharge. The grid rainfall is developed using spatial interpolation on the ground station data. The inverse distance weighted interpolation (IDW) technique was applied for the process. The index of the weighting factor was 2. The spatial distribution of the mean annual rainfall from 1981 to 2010 is shown in Figure 9.6. The observed daily data were broken down to estimate the corresponding hourly rainfall depth applying the diurnal variation presented in Figure 9.5. The estimated hourly data and grid data were compared to check the interpolation process. Several scatter plots are shown in Figure 9.7. The rainfall data in Zaragoza and Muñoz were excluded for the interpolation process. This was because the scatter plots of the observed and gridded data do not match, and scatter plot of the near stations will be affected by the mismatched rainfall data.
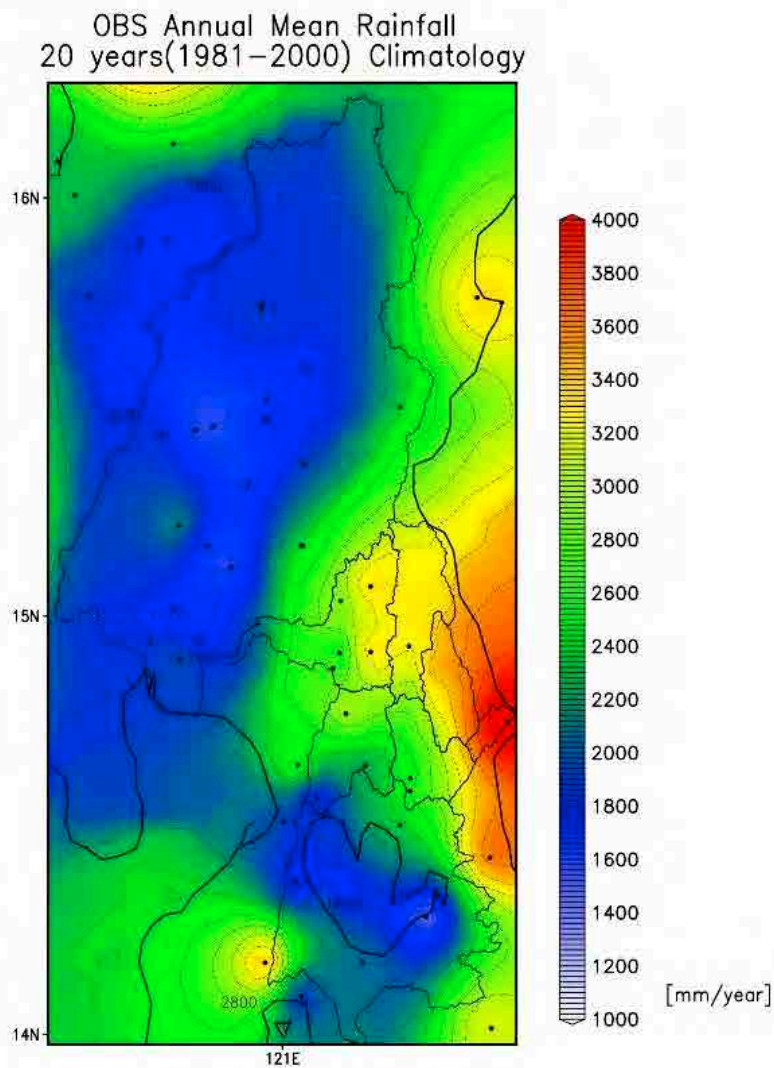
Source: JICA Study Team, based on the observed rainfall record of PAGASA

Figure 9.6   Present Distribution of Annual Rainfall (1981-2000) Based on Observed Data
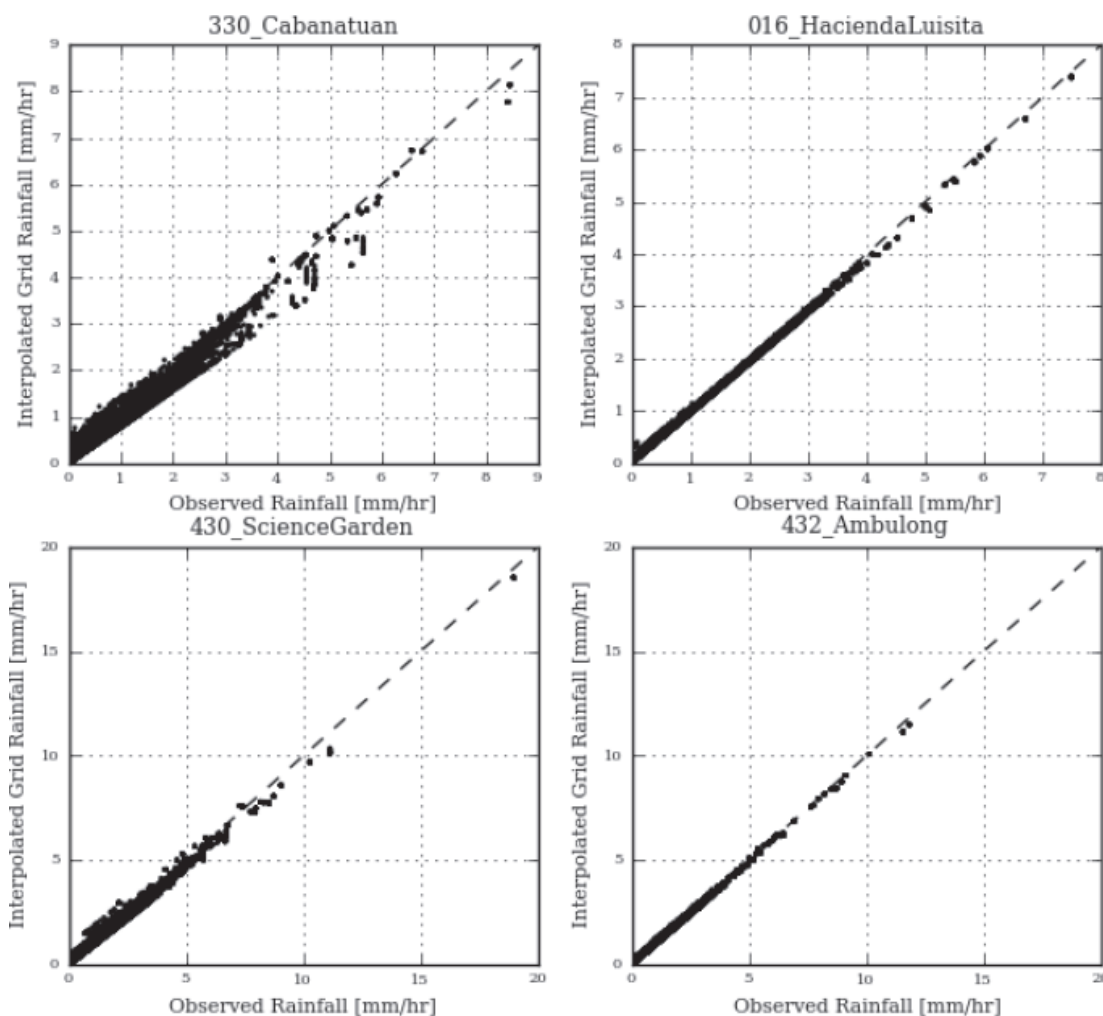
Source: JICA Study Team, based on the observed rainfall record of PAGASA

Figure 9.7   Quality Checks of Observed Rainfall and Interpolation

(2) Temperature

Temporal Downscaling of the Observed Temperature Data:

The variance in the temperature is dominated by the sun. The temporal interpolation from daily maximum and minimum data into hourly temperature was implemented based on an empirical model called the TM model proposed by Carla Cesaraccio (2001), as shown in Figure 9.8.

The procedures of the temporal interpolation of the TM model are as follows:

1) Divide the day into three segments: from the sunrise hour (Hn) to the time of maximum temperature (Hx), from Hx to the sunset hour (H0) and from H0 to the sunrise hour for the next day (Hp).
2) The model is built by two sine-wave functions in the daylight and a square-root decrease in temperature at night.
3) Hn and H0 are determined as a function of the site latitude and the day of the year. Hp is calculated as Hp = Hn + 24.
4) The time of the maximum temperature is set at 4 hours before sunset (Hx = H0 – 4)

The distribution of the mean annual surface temperature is shown in Figure 9.9.
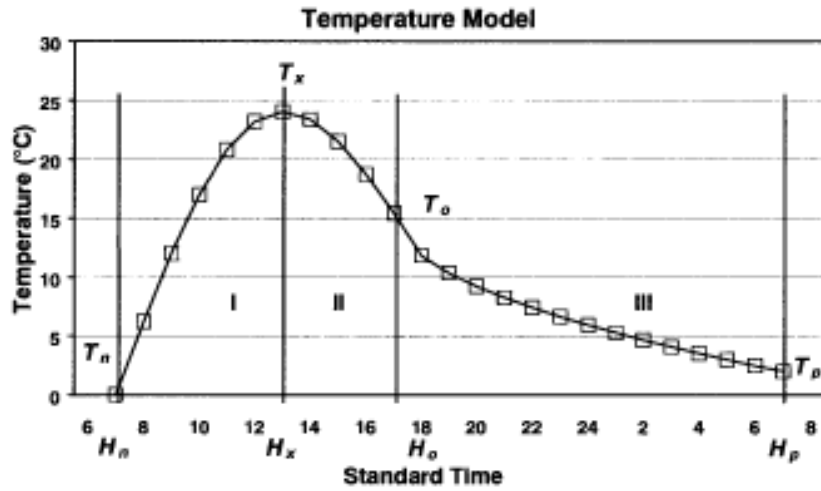
Figure 9.8   Example of Hourly Temperature Calculation by the TM Model
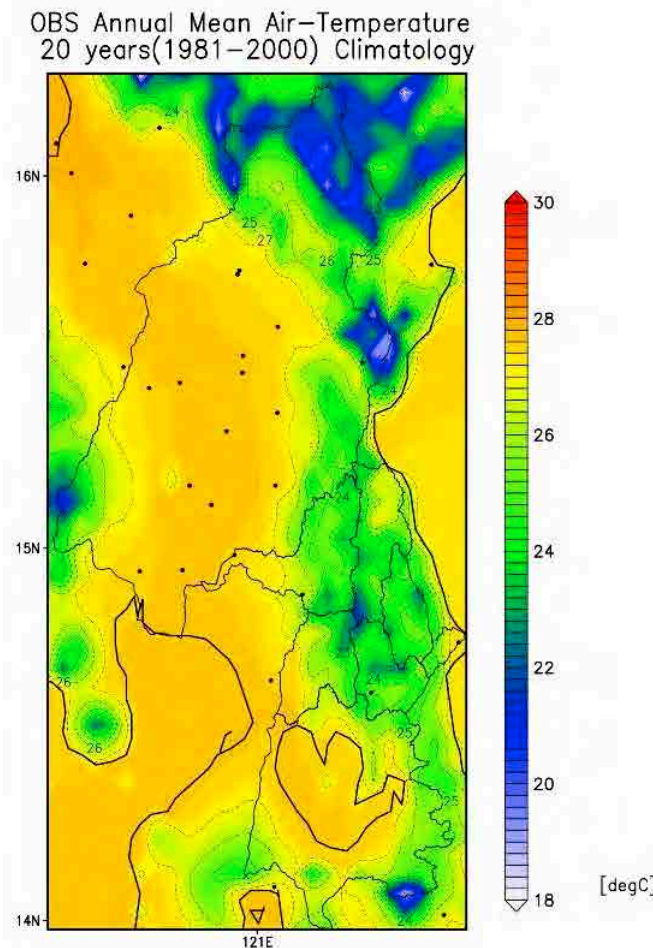
**Figure 9.9   Present Distribution of Annual Mean Surface
Air-Temperature (1981-2000) Based on Observed Data**

(3) Other Parameters

Other forcing meteorological parameters which are required for WEB-DHM are listed in Table 9.4.Surface solar radiation parameters, down welling long wave radiation, short-wave radiation, and cloud fraction were estimated based on the observed sunshine duration, air temperature, and relative humidity. The equations for the parameter estimations were based on those of Yang et al. 2006[1], Yang et al. 2001[2], and Todd and Claude 1998[3]. For the other parameters, such as surface pressure, wind speed, and specific humidity, the Japanese 25-year Reanalysis (JRA25) and JMA Climate Data Assimilation System (JCDAS) were applied.

Table 9.4   Meteorological Forcing Parameters for WEB-DHM

Name	Unit	Data Source
Relative humidity	[%]	Observed station data
Cloud fraction	[%]	Estimated based on observed data: sunshine duration, air temperature, and relative humidity
Long wave radiation	[W/m^2]	"
Short wave radiation	[W/m^2]	"
Pressure	[Pa]	JRA25 dataset
Wind speed	[m/s]	"
Specific humidity	[%]	"

Source: JICA Study Team

9.3 Development of the Basin Model

The target basins of this Study are (i) Pasig-Marikina River basin, (ii) Umiray River basin, (iii) Agos River basin, and (iv) Laguna Lake basin. WEB-DHM was applied for the Pasig-Marikina, Umiray, and Agos River basins. As for the Laguna Lake basin, the SHER model, which is a more simplified runoff model, was applied because of the complex hydraulic conditions of the lake.The hydraulic conductivity of sub-surface soil plays a key role in modeling. Through the modeling of physical characteristics of sub-surface soil, the saturated runoff and sub-surface flow can be estimated precisely.

To determine the best parameters for the target basins, calibration studies by comparing simulated daily discharge with observed daily discharge are necessary. The river gauging stations which are suitable for calibration were selected considering the following: i) location of river network, ii) data availability, and iii) data reliability through checking the annual rainfall-annual runoff ratio and specific discharge.

However, since no river gauging station was available in the Umiray and Agos River basins, the parameters of the runoff model for these two basins could not be calibrated directly. The calibrated parameters for corresponding soil types in the Angat River basin were applied to the model for the adjoining Umiray and Agos River basin. This was so since the model calibration was carried out by the University of Tokyo, which is discussed on another report of this Study, the "Climate Change Impact Assessment and Hydrological Simulation". This

---

[1] Yang, K., Koike, T., and Ye, B. (2006) Improving estimation of hourly, daily, and monthly solar radiation by importing global data sets. Agricultural and Forest Meteorology, 137:43-55.

[2] Yang, K., Koike, T., and Ye, B. (2006). Improving estimation of hourly, daily, and monthly solar radiation by importing global data sets. Agricultural and Forest Meteorology, 137:43-55

[3] Todd M. Crawford and Claude E. Duchon. An improved parameterization for estimating effective atmospheric emissivity for use in calculating daytime down welling long wave radiation, Journal of Applied Meteorology, Volume 38: 474-480, 1998

would be applicable because WEB-DHM is a physically-based model, and the model parameters have physical meanings.

9.3.1 Pasig-Marikina River Basin

(1) Study Area

The Pasig Marikina River runs through Metro Manila. The river connects Laguna Lake with Manila Bay through the Mangahan Floodway and Napindan Channel. The Maggahan Floodway is an artificially constructed waterway that aims to reduce flooding during the rainy season, by bringing excess water to Laguna Lake.

The area considered for simulation in the Pasig-Marikina River basin is shown in Figure 9.10. The total area is around 520 km^2. As shown in Figure 9.10, the lower flat part, where the artificial channels exist, was not included in the modeling. This was because of the difficulty of developing WEB-DHM for such flat areas and the difficulty of modeling complex systems for the artificial facilities. The main purpose of the runoff analysis is to provide the flow condition for the water supply, and the intake facilities are to be proposed in the middle to upper reaches of the river basin. Therefore, the modeled area is enough for this Study, as shown in Figure 9.10.

Source: JICA Study Team, based on SRTM DEM

Figure 9.10   Modeled Area of the Pasig-Marikina River Basin

(2) Topological Process

The Shuttle Radar Topography Mission (SRTM) Digital Elevation Model (DEM) is used to define the target area. The original resolution of the SRTM is about 90 m (0 point and the coordinate system of the grid is aligned with the geographic system).

In order to apply the DEM data for the runoff model, first, the coordinate system was projected into the universal transverse Mercator Coordinate of 51 north. The grid size is re-sampled into 250 m in the projection process. In the original SRTM grid data, there are many missing data grids. The missing data are filled with the average elevation of the surrounding grids of valid data. The re-sampled SRTM DEM data of the basin is shown in item a) of Figure 9.11. The maximum elevation is 1348 m while the minimum elevation is 8 m in the lower reaches of the river basin.

Second, the target basin is divided into smaller scale area using Pfafstetter system. The numbers of the flow intervals in the particular cell of WEB-DHM are specified to represent time lag and concentration processes in the river network according to the distance to the outlet of the sub-basin. The derived hillslope angle is shown in item a) of Figure 9.11, and the divided sub-basins with the flow intervals within the sub-basin are shown in item c) of the same figure.

     a) Digital Elevation Model   b) Slope Angle   c) Sub-basins
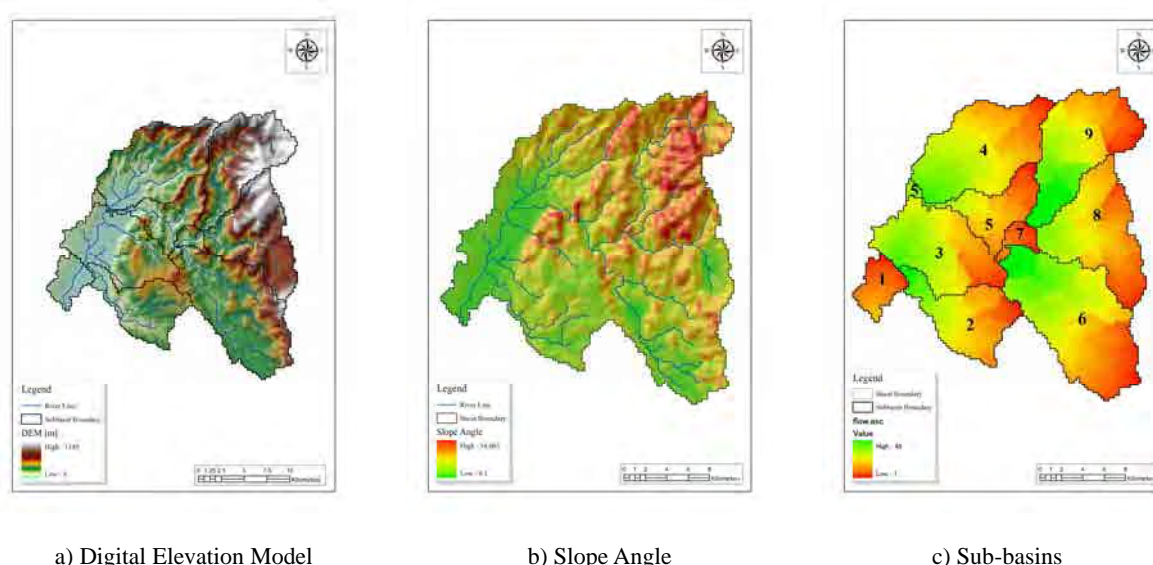
Source: JICA Study Team, based on SRTM DEM

Figure 9.11   Topological Processes for Development of WEB-DHM for Pasig-Marikina River Basin

(3) Land Use and Soil Class

The land surface area of the Pasig Marikina basin is composed of five types of land use and three types of soil class as listed below. Table 9.5 shows the land use and vegetation types using the SiB2 reclassification consist of mostly dwarf trees and shrubs (47%). The dominant soil class using FAO classification in the basin is nitosols (73%), with clay loam as the soil type, as shown in Table 9.6.

Table 9.5   Coverage of Land Use in the Pasig-Marikina River Basin

Land use types using Sib2 reclassification	Coverage [%]
Dwarf trees and shrubs	47.0
Broadleaf deciduous trees	15.2
Agriculture or C3 grasslands	14.1
Shrubs with bare soil	12.5
Short vegetation/C4 grassland	11.2

Source: JICA Study Team, based on DENR dataset

Table 9.6   Coverage of Soil Class in the Pasig-Marikina River Basin

Soil Class using FAO Classification						Coverage [%]
Soil No	Soil Class	Sand %	Silt %	Clay%	Type	
4413	Nitosols	44.78	22.92	32.30	Clay loam	73.1
4478	Cambisols	40.93	25.51	22.55	Clay loam	17.5
4465	Acrisols	48.52	21.77	29.72	Sandy clay loam	9.4

Source: JICA Study Team, based on DENR dataset and FAO dataset

(4) Model Parameters

In the Pasig-Marikina River basin, calibration was conducted by comparing the simulated daily discharges with observed daily discharge. The efficiency criteria of the relative error (RE) and the Nash-Shtcliffe (NS) model efficiency were used to evaluate the performance of the model. Below are the respective equations of each efficiency criteria.

$$NS = 1 - \frac{\sum_{i=1}^{N}(Q_{oi} - Q_{si})^2}{\sum_{i=1}^{N}(Q_{oi} - \overline{Q}_o)^2}$$

$$RE = \frac{\sum_{i=1}^{N}|Q_{si} - Q_{oi}|}{\sum_{i=1}^{N}Q_{oi}}$$

where Q_o is observed discharge; Q_s is simulated discharge; $\overline{Q}_o$ is averaged observed discharge; N is the total number of time-series for comparison.

Calibration in the Pasig-Marikina River basin was done for year 2004. It is difficult to fit the peak flows due to possible limitation of data available for the observed hourly rainfall. As mentioned earlier, the model in this Study was driven by temporal downscaled hourly rainfall instead of observed hourly rainfall. Therefore, calibration was conducted focusing on base flow. As Figure 9.12 shows, WEB-DHM driven by meteorological observations finally simulates the daily discharge at San Jose River Gauging Station with NS of 0.79 and RE of 44.47, indicating good accuracy.

Validation was carried out for the years 1999 to 2006. Figure 9.13 and Figure 9.14 show the results obtained by validated discharges for long-term simulations. The efficiency criterion of the coefficient of determination (R2) was evaluated to be 0.73, which indicates that the model has high accuracy based on the comparison with observed data. Some simulated discharge

data were quite different from observed data, and it is considerable that the observed discharge data has poor quality. In conclusion, this result justified that WEB-DHM is capable of simulating over a climatological period of time.

All model parameters were finally determined by various analysis and simulations. The calibrated parameters for vegetation classes, soil types, and river channels were summarized in Table 9.6 to Table 9.8.
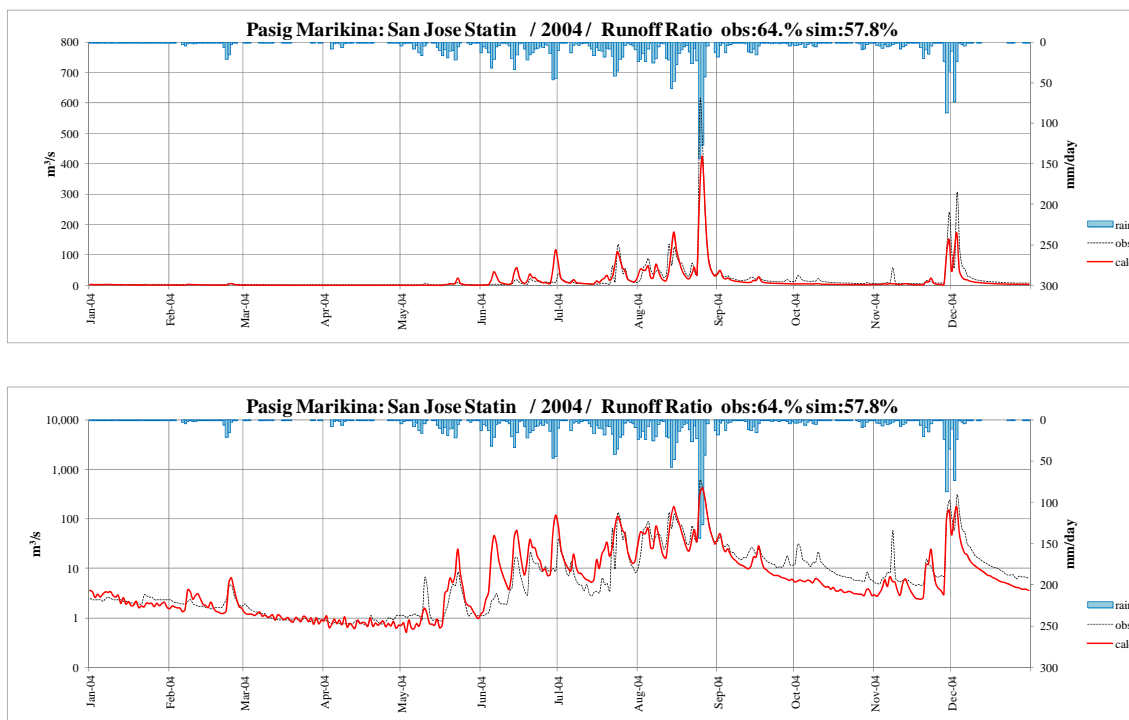
Note: The red line shows simulated discharge; the black dashed line shows observed discharge; and the blue bars show basin average rainfall based on observed data.
Source: JICA Study Team

Figure 9.12   Calibration of San Jose Discharge for 2004, a) Normal Scale and b) Logarithmic Scale
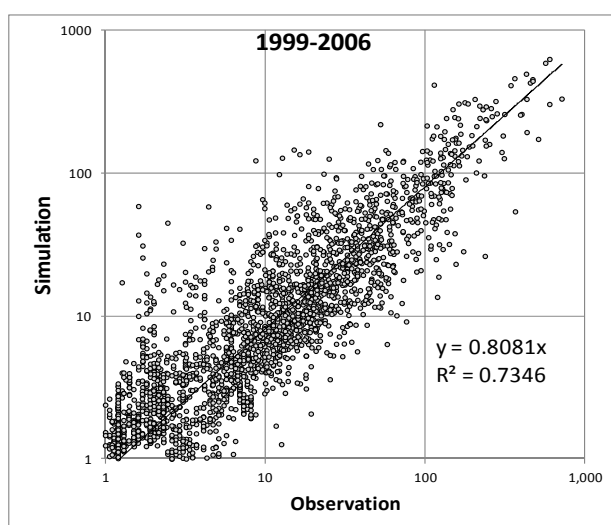
Source: JICA Study Team

Figure 9.13   Scatter Plot of Simulated vs Observed Discharge in San Jose for 1999-2006

Source: JICA Study Team

Figure 9.14   Validation of San Jose Discharge from 1999-2006, Logarithmic Scale

Table 9.7   Calibrated Vegetation Parameters for Pasig-Marikina River Basin

SiB2 Reclassification	coverage [%]	SSTmax [mm]		soil-anisotropic-radiation (anik)		Rooting depth [m]
		SiB2	**calibrate SiB2 * 1**	SiB2	**calibrate SiB2 * 5**	
2-Broadleaf Deciduous Trees	15.17	10	10	10	50	1.5
8-Dwarf trees and Shrubs	46.99	5	5	4	20	1
9-Agriculture or C3 Grasslands	14.13	5	5	3	15	1
7-Shrubs with bare soil	12.49	5	5	1	5	1
6-Short vegetation/C4 grassland	11.22	5	5	3	15	1

Source: JICA Study Team

Table 9.8   Calibrated Soil Parameters for Pasig-Marikina River Basin

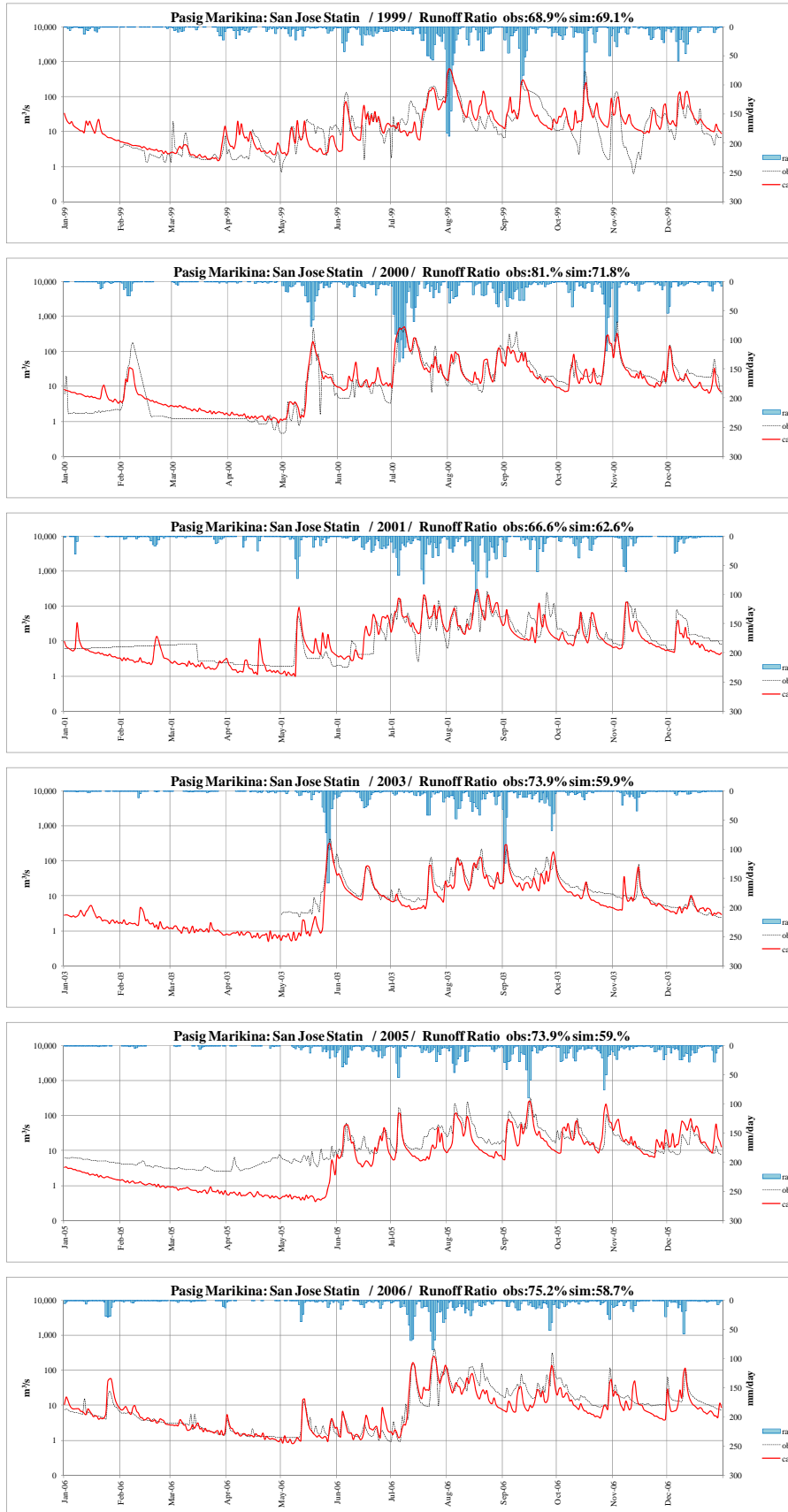| Classification		coverage	Soil water parameters								
soil code	Soil Class (FAO)	[%]	theta_s	theta_r	alpha	n	ks1		ks2		ksg	GWcs
							fao	**calibrate fao * 10**	ks1 * 0.1	fao	**calibrate fao * 100**	
4413	NITOSOLS	73.1	0.438	0.069	0.021	1.484	13.843	138.428	1.384	0.692	69.214	0.15
4478	CAMBISOLS	17.5	0.447	0.076	0.015	1.467	8.972	89.724	0.897	0.449	44.862	0.15
4465	ACRISOLS	9.4	0.464	0.072	0.021	1.494	24.473	244.728	2.447	1.224	122.364	0.15

Source: JICA Study Team

Table 9.9   Calibrated River Channel Parameters for Pasig-Marikina River Basin

sub_basin ID	width_min	width_max	height_min	height_max	roughness_min	roughness_max	roughness_n
					calibrate	**calibrate**	**caliblate**
900	10	50	2	2	0.5	0.5	0.05
800	10	50	2	2	0.5	0.5	0.05
700	50	50	3	4	0.5	0.5	0.05
600	10	50	3	3	0.5	0.5	0.05
500	20	50	3	4	0.5	0.5	0.05
400	10	50	3	3	0.5	0.5	0.05
300	50	80	3	4	0.5	0.5	0.05
200	10	50	3	3	0.5	0.5	0.05
100	80	100	3	4.5	0.5	0.5	0.05

Source: JICA Study Team

9.3.2   Umiray River Basin

(1) Study Area

Umiray River flows down toward the north and drains out to the Pacific Ocean. The total area considered for simulation in the Umiray River basin is 628 km^2. A part of the Umiray River runoff is transferred to the Angat Reservoir via the Umiray-Angat transbasin diversion channel. The simulation was conducted under the natural conditions with no artificial facilities.

(2) Topological Process

The target area was defined and divided into sub-basins in the same way as shown in the case of Pasig-Marikina River basin.   The re-sampled SRTM DEM of the Umiray River basin is

shown in item a) of Figure 9.15. The maximum elevation is 1428 m while the minimum elevation is almost 0 m at the coast. The derived hillslope angle is shown in item a) of Figure 9.15, and the divided sub-basin with the flow intervals within the sub-basin is shown in item c) of the same figure.

a) Digital Elevation Model   b) Slope Angle   c) Sub-basins
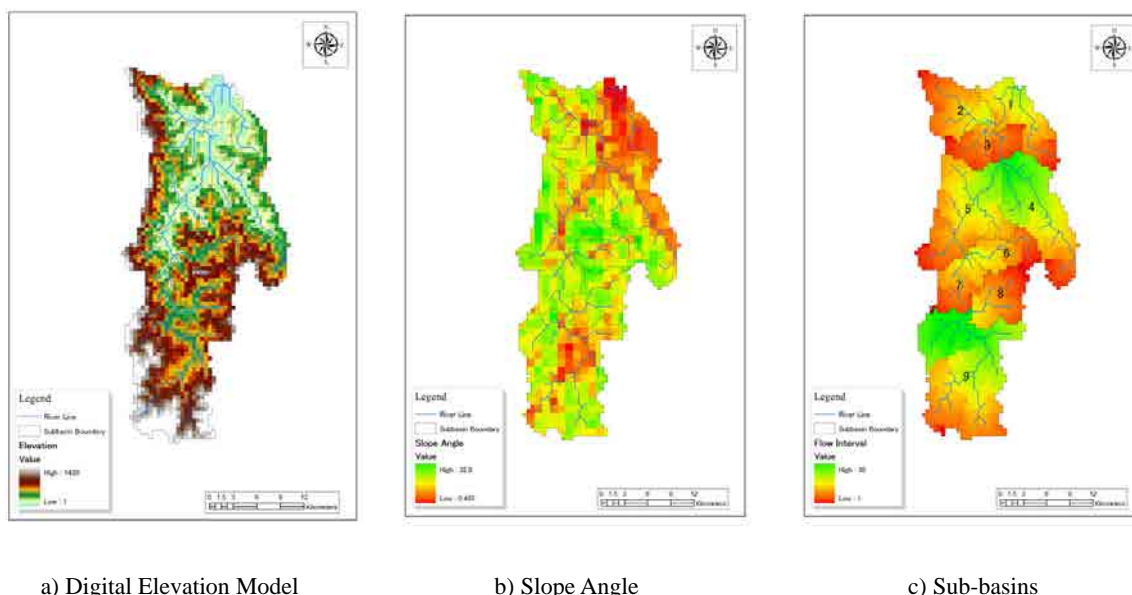
Source: JICA Study Team, based on SRTM DEM

Figure 9.15   Topological Processes for Development of WEB-DHM for Umiray River Basin

(3) Land Use and Local Soil

The land surface area of the Umiray River basin is covered by five types of land use and five types of soil class as listed below. As shown in Table 9.9, land use and vegetation types based on SiB2 reclassification consist mostly of broadleaf deciduous trees (95.7%). The dominant soil classes according to the FAO classification in the basin are nitosols (67.3%) and acrisols (29.4%), with clay loam and sandy clay loam as soil types.

Table 9.10   Coverage of Land Use in the Umiray River Basin

Land Use using Sib2 Reclassification	Coverage [%]
Broadleaf deciduous trees	95.7
Agriculture or C3 grasslands	3.7
Dwarf trees and shrubs	0.5
Shrubs with bare soil	0.04
Short vegetation/C4 grassland	0.04

Source: JICA Study Team, based on DENR dataset

Table 9.11   Coverage of Soil Class in Umiray River Basin

Soil Class using FAO Classification						Coverage [%]
Soil No	Soil Class	Sand %	Silt %	Clay%	Type	
4413	Nitosols	44.78	22.92	32.30	Clay loam	36.9
4546	Nitosols	37.61	24.33	38.06	Clay loam	30.4
4465	Acrisols	48.52	21.77	29.72	Sandy clay loam	29.4
4504	Gleysols	44.05	22.92	33.02	Clay loam	3.0
4537	Luvisols	46.47	23.01	30.52	Sandy clay loam	0.3

Source: JICA Study Team, based on DENR and FAO datasets

(4) Model Parameters

There is no observed data which can be used to calibrate the parameters of Umiray River basin. Hence, the calibrated parameters of corresponding soil types in the Angat River basin which were given by the University of Tokyo were applied. The parameters for each vegetation classes, soil types, and rivers are summarized in Tables 9.11 to 9.13.

Table 9.12　Calibrated Vegetation Parameters for Umiray River Basin

SiB2 Reclassification	coverage [%]	SSTmax [mm]		soil-anisotropic-radiation (anik)		Rooting depth [m]
		SiB2	calibrate SiB2 * 3	SiB2	calibrate SiB2 * 5	
2-Broadleaf Deciduous Trees	95.74	10	30	10	50	1.5
9-Agriculture or C3 Grasslands	3.69	5	15	3	15	1
8-Dwarf trees and Shrubs	0.49	5	15	4	20	1
6-Short vegetation/C4 grassland	0.04	5	15	3	15	1
7-Shrubs with bare soil	0.04	5	15	1	5	1

Source: JICA Study Team

Table 9.13　Calibrated Soil Parameters for Umiray River Basin

Classification		coverage	Soil water parameters									
soil code	Soil Class (FAO)	[%]	theta_s	theta_r	alpha	n	ks1		ks2	ksg		GWcs
							fao	calibrate fao * 1	ks1 * 0.1	fao	calibrate fao * 10	
4413	NITOSOLS	36.9	0.438	0.069	0.021	1.484	13.843	13.843	1.384	0.692	6.921	0.15
4546	NITOSOLS	30.4	0.478	0.080	0.018	1.435	20.646	20.646	2.065	1.032	10.323	0.15
4465	ACRISOLS	29.4	0.464	0.072	0.021	1.494	24.473	24.473	2.447	1.224	12.236	0.15
4504	GLEYSOLS	3.0	0.449	0.079	0.015	1.450	8.811	8.811	0.881	0.441	4.405	0.15
4537	LUVISOLS	0.3	0.432	0.070	0.018	1.486	11.355	11.355	1.135	0.568	5.678	0.15

Source:　JICA Study Team

Table 9.14　Calibrated River Parameters for Umiray River Basin

sub_basin ID	width_min	width_max	height_min	height_max	roughness_min	roughness_max	roughness_n
					calibrate	calibrate	caliblate
900	10	50	2	2	0.25	0.25	0.045
800	10	50	2	2	0.25	0.25	0.045
700	20	50	3	4	0.25	0.25	0.045
600	10	50	3	3	0.25	0.25	0.045
500	50	50	3	4	0.25	0.25	0.045
400	10	50	3	3	0.25	0.25	0.045
300	50	80	3	4	0.25	0.25	0.045
200	10	50	3	3	0.25	0.25	0.045
100	80	120	3	4.5	0.25	0.25	0.045

Source: JICA Study Team

9.3.3　Agos River Basin

(1) Study Area

The Agos River basin includes the Kaliwa and Kanan River basins. The Kanan River basin is located in the southwestern part while the Kaliwa River basin is in the northeastern part. After the confluence of Kaliwa and Kanan rivers, the mainstream is then named as the Agos River, which flows eastward and drains out the Pacific Ocean. The total area considered for simulation on the Agos River basin is 950 km^2.

(2) Topological Process

The target area was defined and divided into sub-basins in the same way as shown in the case of the Pasig-Marikina River basin. The re-sampled SRTM DEM of the Agos River basin is shown in item a) of Figure 9.16. The maximum elevation is 1489 m, which is located in the Kaliwa River basin, while the minimum elevation is almost 0 m at the coast. The derived hillslope angle is also shown in item a), and the divided sub-basin with the flow intervals within the sub-basin is shown in item c) of the same figure.

| a) Digital Elevation Model | b) Slope Angle | c) Sub-basins |
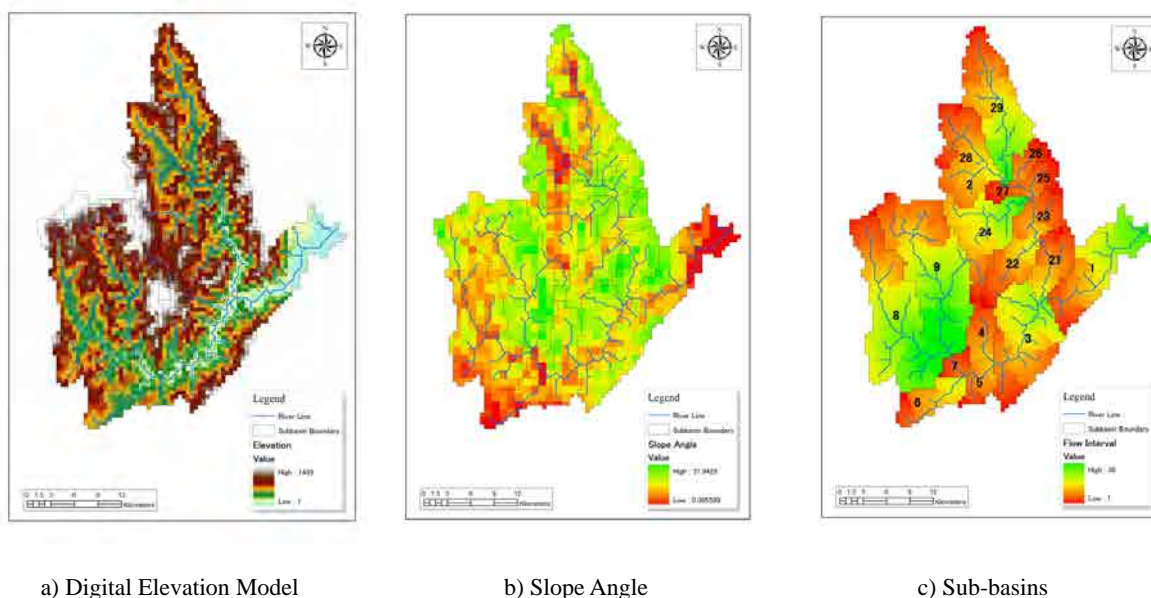
Source: JICA Study Team, based on SRTM DEM

Figure 9.16   Topological Processes for Development of WEB-DHM for the Agos River Basin

(3) Land Use and Local Soil

The land surface area of the Agos River basin is covered by four types of land use types and two soil classes. As shown in Table 9.15, land use and vegetation types using the SiB2 reclassification consist mostly of broadleaf deciduous trees (75.3%). The dominant soil classes using FAO classification in the basin are Acrisols (64.9%) and Nitosols (35.1%), and the soil types are sandy clay loam and clay loam.

Table 9.15   Coverage of Land Use in Agos River Basin

Land Use using Sib2 Reclassification	Coverage [%]
Broadleaf deciduous trees	75.3
Dwarf trees and shrubs	22.3
Agriculture or C3 grasslands	2.2
Short vegetation or C4 grassland	0.2

Source: JICA Study Team, based on DENR dataset

Table 9.16   Coverage of Soil Class in Agos River Basin

Soil Class using FAO Classification						Coverage [%]
Soil No	Soil Class	Sand %	Silt %	Clay%	Type	
4465	Acrisols	48.52	21.77	29.72	Sandy clay loam	64.9
4413	Nitosols	44.05	22.92	33.02	Clay loam	35.1

Source: JICA Study Team with DENR dataset and FAO dataset

(3) Model Parameters

There were no observed data which can be used for calibrating the parameters for the Agos River basin. Therefore, the calibrated parameters for the Angat River basin which were given by the University of Tokyo were applied. The parameters for each vegetation classes, soil types, and rivers are summarized in Tables 9.17 to Table 9.19.

Table 9.17   Calibrated Vegetation Parameters for the Agos River Basin

SiB2 Reclassification	coverage [%]	SSTmax [mm]		soil-anisotropic-radiation (anik)		Rooting depth [m]
		SiB2	calibrate SiB2 * 3	SiB2	calibrate SiB2 * 5	
2-Broadleaf Deciduous Trees	75.26	10	30	10	50	1.5
8-Dwarf trees and Shrubs	22.30	5	15	4	20	1
9-Agriculture or C3 Grasslands	2.21	5	15	3	15	1
6-Short vegetation/C4 grassland	0.24	5	15	3	15	1

Source: JICA Study Team

Table 9.18   Calibrated Soil Parameters for the Agos River Basin

Classification		coverage	Soil water parameters									
soil code	Soil Class (FAO)	[%]	theta_s	theta_r	alpha	n	ks1		ks2		ksg		GWcs
							fao	calibrate fao * 1	ks1 * 0.1	fao	calibrate fao * 10	
4465	ACRISOLS	64.9	0.464	0.072	0.021	1.494	24.473	24.473	2.447	1.224	12.236	0.15
4413	NITOSOLS	35.1	0.438	0.069	0.021	1.484	13.843	13.843	1.384	0.692	6.921	0.15

Source: JICA Study Team

Table 9.19   Calibrated River Parameters for the Agos River Basin

sub_basin ID	width_min	width_max	height_min	height_max	roughness_min	roughness_max	roughness_n
					calibrate	calibrate	caliblate
900	10	50	2	2	0.25	0.25	0.045
800	10	50	2	2	0.25	0.25	0.045
700	50	50	3	4	0.25	0.25	0.045
600	10	50	3	3	0.25	0.25	0.045
500	50	50	3	4	0.25	0.25	0.045
400	10	50	3	3	0.25	0.25	0.045
300	50	80	3	4	0.25	0.25	0.045
290	10	40	2	3	0.25	0.25	0.045
280	10	40	2	3	0.25	0.25	0.045
270	50	50	3	3	0.25	0.25	0.045
260	10	40	2	3	0.25	0.25	0.045
250	10	40	2	3	0.25	0.25	0.045
240	10	40	2	3	0.25	0.25	0.045
230	40	50	3	4	0.25	0.25	0.045
220	10	40	2	3	0.25	0.25	0.045
210	50	80	3	4	0.25	0.25	0.045
100	80	120	3	4.5	0.25	0.25	0.045

Source: JICA Study Team

9.3.4   Laguna Lake Basin

(1) Study Area

Laguna Lake is a large shallow freshwater body in the heart of Southern Luzon Island with an aggregate area of about 911 km^2. The lake has an average depth of 2.8 m and its excess water is drained to Manila Bay via the Pasig River.

The main objective of rainfall-runoff analysis for Laguna Lake basin is to evaluate the water resources flowing into the lake from the related catchments surrounding the lake. There are many basins surrounding the lake and the nearby areas are very flat, which makes it difficult to perform topological pre-process for WEB-DHM. Therefore, the SHER model was applied for the rainfall-runoff modeling which can be utilized for such flat areas and can handle many catchments all together.

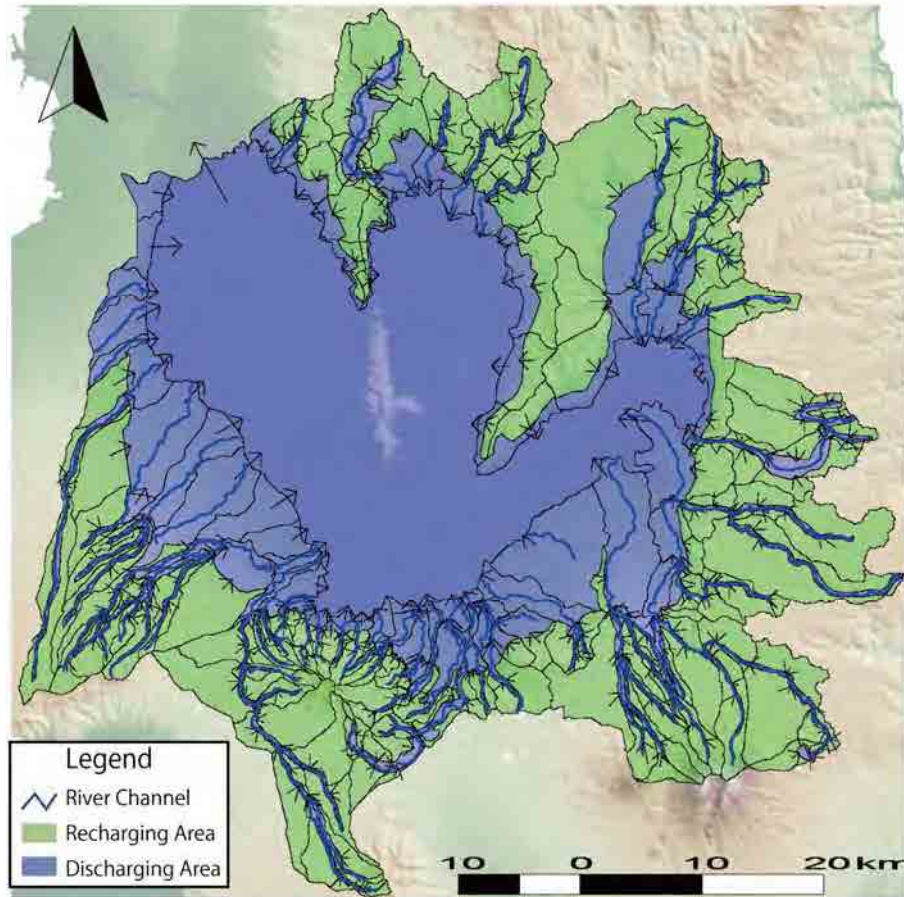(2) Delineation of SHER Blocks

The discharging and recharging areas are divided for the SHER blocks. Recharging area is where water from precipitation is transmitted downwards to an aquifer. The discharging area is the opposite of recharging area. These are located where groundwater moves from the aquifer to surface. Groundwater discharge occurs where the water table intersects the land surface, and river channels appear when the groundwater table is higher than the bottom of the channel. High areas, such as hills or plateaus, are typically where aquifers are recharged and low areas, such as river valleys, are where aquifers discharged. However, in many cases, the aquifer level is lower than the river bed, and the river water recharges the aquifer. Such areas were also treated as discharging areas in the SHER model, because the groundwater table rises during rainy season and discharges the excess.

The total number of SHER blocks was 345 for the whole area of Laguna Lake basin as illustrated in Figure 9.17.
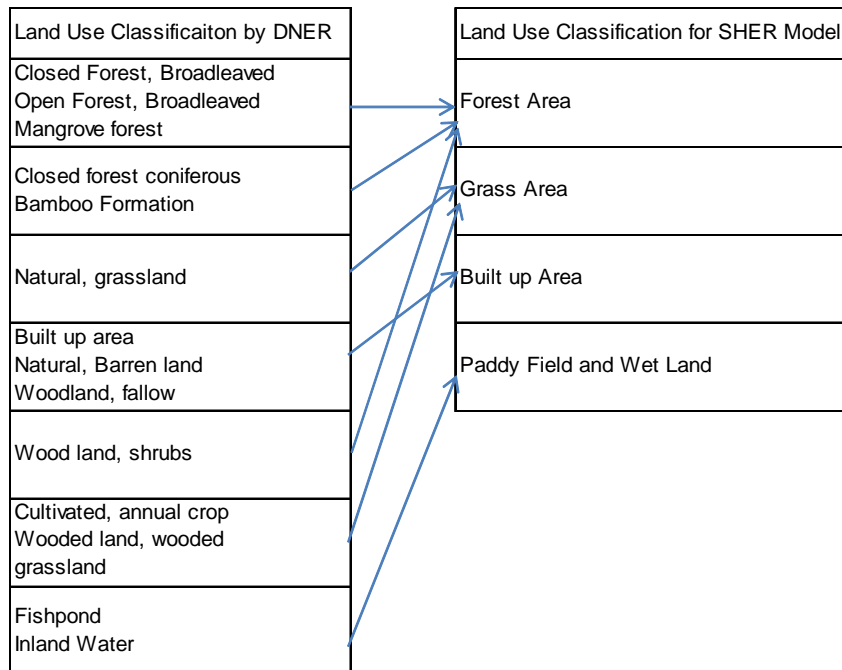
(3) Land Use and Impervious Area

The land use condition plays a key role in setting the soil parameter of surface cover. The land use categories of DENR were re-classified for the SHER model from the standpoint of surface soil status. For example, the soil on forest and agricultural areas can be regarded as having the same status in view of the hydraulic conductivity because the surface soil on these areas has large porosity. The paddy field, mangrove area, and wetland area can be put in the same soil status for hydrological model parameters, since the surface soil on those areas is composed of silt or clay where hydraulic conductivity is very small. The re-classification of the land use category for SHER model is shown in Figure 9.18.

The ratio of impervious area to the land use category of "build-up area" was evaluated as 0.7 by measuring the area covered in pavement and roof in the urban area using the aerial imagery of Google Earth. The hydrological process in impervious area is quite different from the previous area. It is important to set the ratio in SHER model, because the runoff ratio is significantly affected by the impervious area. The ratios of classified land use are shown in Figure 9.19.
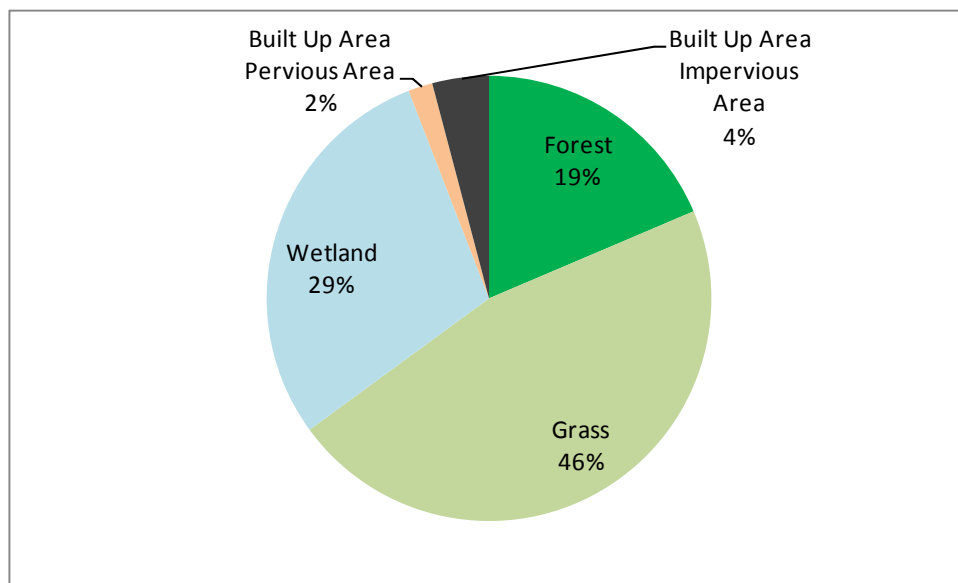
Source: JICA Study Team

Figure 9.17   Delineation of SHER Blocks for Laguna Lake Basin

Source: JICA Study Team

Figure 9.18   Re-classification of Land Use for SHER Model

Source: JICA Study Team

Figure 9.19   Ratios of Land Use Area and Impervious Area for Laguna Lake Basin

(4) Sub-surface Soil

The modeling of hydraulic conductivity of sub-surface soil is very important. Through the modeling of physical characteristics of sub-surface soil, the saturated runoff and the sub-surface flow can be estimated precisely.

By overlapping with the aforementioned land use distribution, the surface soil type was divided into 31 types. There are six soil types as classified by FAO. The list of soil type classification is shown in Table 9.20.

(5) River Flow Observed Data for Calibration

There were only three river gauging stations, namely Mayor, San Cristobal, and San Juan, that have observed river discharge data. The observed data in San Cristobal was found to have errors, and was excluded in the calibration works. The location of the river gauging stations is shown in Figure 9.20.

Table 9.20   Soil Type Classification for Laguna Lake Basin SHER Model

No	Soil Name
1	ForestNITOSOLS_RechargingArea
2	ForestACRISOLS_RechargingArea
3	ForestCAMBISOLS_RechargingArea
4	ForestGLEYSOLS_RechargingArea
5	ForestLUVISOLS_RechargingArea
6	ForestVERTISOLS_RechargingArea
7	GlassNITOSOLS_RechargingArea
8	GlassACRISOLS_RechargingArea
9	GlassCAMBISOLS_RechargingArea
10	GlassGLEYSOLS_RechargingArea
11	GlassLUVISOLS_RechargingArea
12	GlassVERTISOLS_RechargingArea
13	CLAY
14	BuiltUp_NITOSOLS
15	BuiltUp_ACRISOLS
16	BuiltUp_CAMBISOLS
17	BuiltUp_GLEYSOLS
18	BuiltUp_LUVISOLS
19	BuiltUp_VERTISOLS
20	ForestNITOSOLS_DischargingArea
21	ForestACRISOLS_DischargingArea
22	ForestCAMBISOLS_DischargingArea
23	ForestGLEYSOLS_DischargingArea
24	ForestLUVISOLS_DischargingArea
25	ForestVERTISOLS_DischargingArea
26	GlassNITOSOLS_DischargingArea
27	GlassACRISOLS_DischargingArea
28	GlassCAMBISOLS_DischargingArea
29	GlassGLEYSOLS_DischargingArea
30	GlassLUVISOLS_DischargingArea
31	GlassVERTISOLS_DischargingArea

Source: JICA Study Team
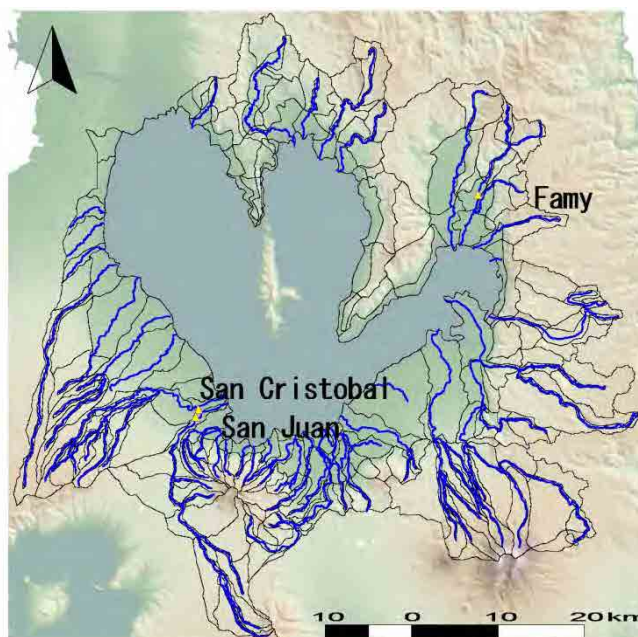
Source: JICA Study Team

Figure 9.20   Location of River Gauging Station in Laguna Lake Basin